7
Zonal mean state of the atmosphere

Any observer of the atmosphere must be struck by the fact that it is always in motion
John Dutton (1986), ***The Ceaseless Wind***. Dover edition, p. 8.

Getting a feel for the character of the solution in different circumstances.
Analysis of real physical problems is usually quite complicated, and any particular physical situation may be too complicated to analyze directly by solving the differential equation. But one can still get a very good idea of the behavior of a system if one has some feel for the character of the solution in different circumstances.
Richard Feynman, 1963: ***The Feynman*** **Lectures on Physics.** Addison-Wesley Publishing Company. Section 2-1

7.1 Introduction: the polar vortex

The best theoretical framework for the desciption of the dynamical structure of the atmosphere is one which divides this dynamical structure into the following **three interacting components**: **(1)** a **"primary", zonally symmetric, zonal circulation**, **(2)** a **"secondary", zonally symmetric, meridional circulation** (the Hadley- and Ferrel cells), and **(3)** **eddies and waves, which are zonally asymmetric**. This chapter describes the observed "primary", zonally symmetric, zonal circulation, including the zonal mean jets. The **primary circulation**, outside the deep tropics, i.e. the polar vortex, is always very close to a steady state of **thermal wind balance**, despite the continuous presence of eddies, which bring it out of balance by poleward transport of mass (heat) and vorticity (momentum). The "secondary" circulation exists in order to maintain the primary circulation in thermal wind balance.

Box 7.1 Summary of some important definitions and equations

This **box** provides an overview of "primitive" equations in isentropic coordinates, which are derived in **section 1.23** of these lecture notes and used in this chapter.

Potential temperature, θ, is defined as

$$\theta = T\left(\frac{p_{ref}}{p}\right)^{\kappa}, \tag{1}$$

where T is temperature, $\kappa=R/c_p$, R is the specific gas constant for dry air, c_p is the heat capacity at constant pressure, and p_{ref}=1000 hPa. The two horizontal components of the equation of motion in isentropic coordinates (i.e with θ as a vertical coordinate) are

$$\frac{du}{dt} = \frac{\partial u}{\partial t} + u\left[\frac{\partial u}{\partial x}\right]_\theta + v\left[\frac{\partial u}{\partial y}\right]_\theta + \frac{d\theta}{dt}\frac{\partial u}{\partial \theta} = -\left[\frac{\partial \Psi}{\partial x}\right]_\theta + fv + \frac{uv\tan\phi}{a} + F_x, \tag{2}$$

$$\frac{dv}{dt} = \frac{\partial v}{\partial t} + u\left[\frac{\partial v}{\partial x}\right]_\theta + v\left[\frac{\partial v}{\partial y}\right]_\theta + \frac{d\theta}{dt}\frac{\partial v}{\partial \theta} = -\left[\frac{\partial \Psi}{\partial y}\right]_\theta - fu - \frac{u^2\tan\phi}{a} + F_y. \tag{3}$$

Here, F_x and F_y are yet unidentified frictional forces and Ψ is the **isentropic stream function** (or Montgomery streamfunction), defined as

$$\Psi = c_p T + gz, \tag{4}$$

where and g is the acceleration due to gravity.
The vertical balance of forces is represented by the **hydrostatic relation**:

$$\frac{\partial \Psi}{\partial \theta} \equiv \Pi, \tag{5}$$

where the **Exner function** is defined as

$$\Pi \equiv c_p\left(\frac{p}{p_{ref}}\right)^{\kappa}. \tag{6}$$

Relative vorticity, ζ_θ, in isentropic coordinates is

$$\zeta_\theta = \left(\frac{\partial v}{\partial x}\right)_\theta - \left(\frac{\partial u}{\partial y}\right)_\theta. \tag{7}$$

Potential vorticity (PV) in isentropic coordinates is

$$Z_\theta \equiv \frac{\zeta_\theta + f}{\sigma} = -g\left(\zeta_\theta + f\right)\frac{\partial \theta}{\partial p}\ , \qquad (8)$$

where σ is **isentropic density**, defined by

$$\sigma = -\frac{1}{g}\frac{\partial p}{\partial \theta} \qquad (9)$$

The equation **mass conservation** is isentropic coordinates is

$$\frac{\partial \sigma}{\partial t} + \left(\frac{\partial \sigma u}{\partial x}\right)_\theta + \left(\frac{\partial \sigma v}{\partial y}\right)_\theta + \frac{\partial}{\partial \theta}\left(\sigma \frac{d\theta}{dt}\right) = 0\,. \qquad (10)$$

The **potential vorticity equation** (derived from eqs. 2, 3 and 10, neglecting the curvature terms in eqs. 2 and 3, is

$$\frac{dZ_\theta}{dt} = Z_\theta \frac{\partial}{\partial \theta}\frac{d\theta}{dt} + \frac{1}{\sigma}\frac{\partial u}{\partial \theta}\frac{\partial}{\partial y}\frac{d\theta}{dt} - \frac{1}{\sigma}\frac{\partial v}{\partial \theta}\frac{\partial}{\partial x}\frac{d\theta}{dt} + \frac{1}{\sigma}\left(\frac{\partial F_y}{\partial x} - \frac{\partial F_x}{\partial y}\right), \qquad (11)$$

If $d\theta/dt$=0 (**adiabatic conditions**) and F_x=0 and F_y=0:

$$\frac{dZ_\theta}{dt} = 0\ . \qquad (12)$$

In other words, potential vorticity is materially conserved under adiabatic and frictionless conditions.

Figure 7.1 shows the zonal mean zonal wind, $[u]$[1], the zonal mean potential vorticity, $[Z_\theta]$, (eq. 8 in **Box 7.1**) and the zonal mean pressure, $[p]$, as a function of latitude and potential temperature in January and July, according to the COSPAR International Reference Atmosphere (CIRA)[2]. Remember that surfaces of constant potential temperature (**isentropic surfaces**) are material surfaces in adiabatic conditions. Potential vorticity is also materially conserved in adiabatic and frictionless conditions. The most interesting isentropic surfaces are those corresponding to "Middleworld", approximately between 310 K and 380 K. These surfaces intersect the dynamical tropopause, which is defined as the the ±2 Potential Vortcity Unit (PVU)[3] contour. In the Middleworld the dynamical tropopause separates stratospheric air in the middle latitudes form tropospheric air in the tropics.

[1] Square brackets indicate a zonal mean, i.e a mean long a circle of constant latitude.

[2] Fleming, E. L., Chandra, S., Barnett, J. J. and Corney, M., 1990: Zonal Mean Temperature, Pressure, Zonal Wind, and Geopotential Height as Functions of Latitude. **Advances in Space Research, 10**, No. 12, 11-59.

[3] 1 PVU = 10^{-6} K m^{2}kg^{-1}s^{-1}

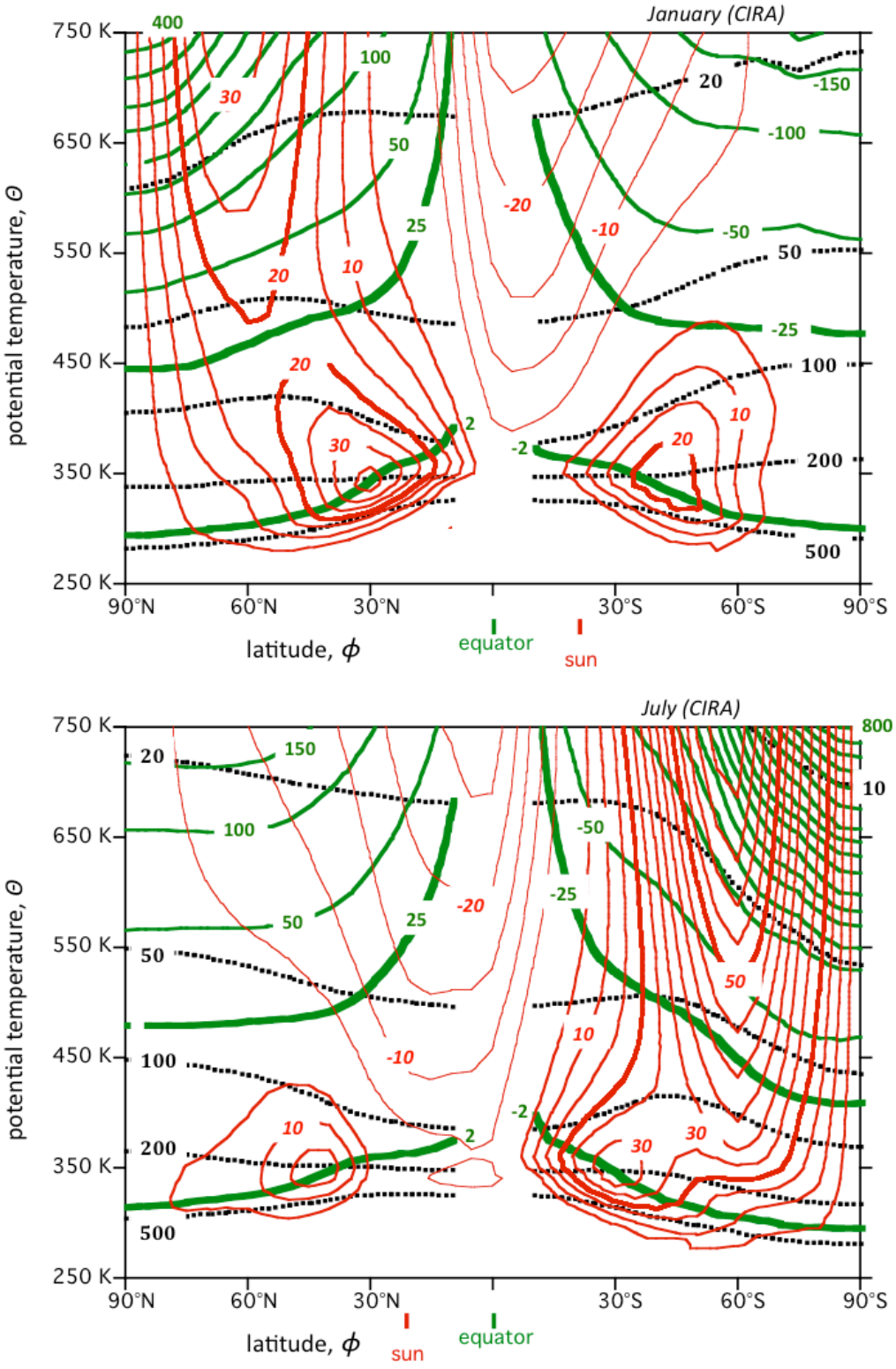

FIGURE 7.1. The zonal average, monthly average of zonal wind, $[u]$ (red contours, labeled in m s^{-1}), of potential vorticity $[Z_\theta]$ (eq. 8, **Box 7.1**) (green contours, labeled in PVU; interval is 50 PVU [1 PVU=1 K $m^2kg^{-1}s^{-1}$] for absolute values greater than 50) and pressure, $[p]$ (black dashed contours, labeled in hPa) as a function of potential temperature and latitude according to the COSPAR International Reference Atmosphere (CIRA) for January and July. The monthly average overhead position of the sun is indicated in red below each figure.

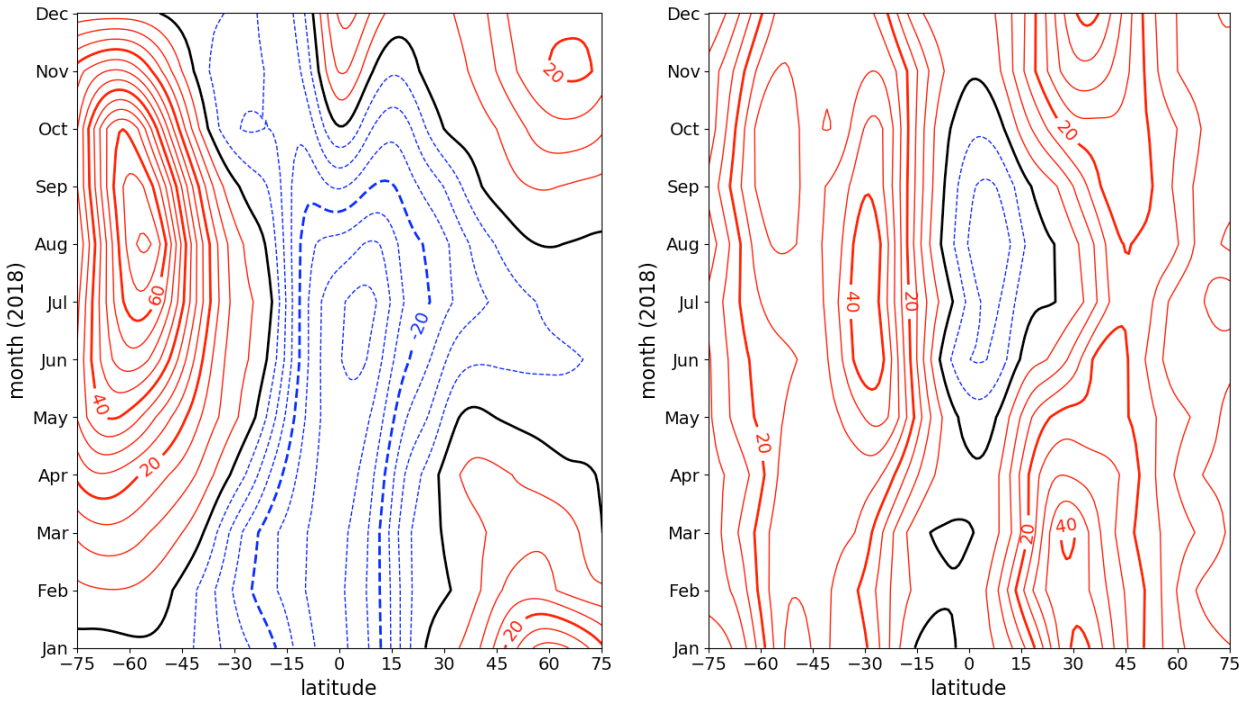

FIGURE 7.2. Hovmöller diagram showing the zonal mean zonal wind velocity, $[u]$, at θ=600 K (left panel) and at θ=350 K (right panel) as a function of latitude and month for the year 2018. The analysis is based on monthly mean of daily mean ERA-Interim values of $[u]$ (https://apps.ecmwf.int). Contour interval is 5 m s^{-1}. Labels in units of m s^{-1}. The black contour corresponds to 0 m/s.

The zonal mean zonal wind exhibits a seasonal cycle (**figures 7.1** and **7.2**), which is especially strong in the stratosphere. In winter two eastward jets can be distinguished: a **subtropical jet** at about 30° latitude and 350 K and a **stratospheric polar night jet** at about 60° latitude and above 500 K in the Northern Hemisphere and above 400 K in the Southern Hemisphere. In summer the subtropical jet weakens and shifts polewards while the stratosphere jet reverses direction, becoming westward and very weak. In other words, in summer an **anticyclonic circumpolar vortex** is observed in the stratosphere, while a **cyclonic circumpolar vortex** remains in the troposphere and lower stratosphere. The **wind-reversal in spring and autumn** in the stratosphere (e.g. at 600 K) is due to the interplay of "planetary wave drag" and radiative heating and cooling. This complex nonlinear interaction will be explored in **chapter 12**.

Figure 7.3 shows maps of potential vorticity, Z_θ (PV), defined in eq. 8 of Box 7.1, and of the x-component of the wind velocity, u, in the layers θ=330-370 K (left) and θ=600-700 K (right) in the Northern Hemisphere on January 8, 2009. The first layer is located at tropopause level (about 10 km above sea level). The second layer is located at about 20 hPa (25 km above sea level). In both layers we observe high PV-values in a reasonably circular area centred over the pole. The outer boundary of this area is characterised by a strong meridional PV-gradient in both layers. In the lower layer (at 330-370 K) this PV-gradient is observed approximately at 20-30°N. This corresponds to the poleward edge of the tropical Hadley circulation. In the upper layer (at 600-700 K) this PV-gradient is observed approximately at 60-65°N. This corresponds approximately to the edge of the Polar night. In the Polar night the atmosphere cools by emission of radiation. There is no compensating diabatic heating by Solar radiation.

In the winter hemisphere, cooling by radiation in the extra-tropics is manifest principally as a net divergence of the downwelling cross-isentropic mass flux. Mass crosses isentropes and is ultimately stored in the "Underworld" (the layer below 300 K). In this way a negative

isentropic density anomaly develops above 300 K especially over the Polar Cap. This negative isentropic density anomaly is observed in the upper panels of **figure 7.4**. Since potential vorticity is inversely proportional to isentropic density, the negative isentropic density anomalies are manifest as positive potential vortcity anomalies (**figure 7.3**). In this chapter it is shown that thermal wind balance dictates that a negative isentropic density anomaly should be accompanied by a positive vorticity anomaly (see also **section 1.33**). This is verified in the lower panels of **figure 7.4**.

In this chapter a deep understanding of the thermal and dynamical structure of the zonally symmetric component of the circumpolar flow is developed from one single equation, i.e. the **thermal wind balance equation**, which can be expressed in terms of **potential vorticity**. Solutions of this so-called **potential vorticity (PV)-inversion equation** reveal how large-scale patterns of wind, temperature and pressure are interconnected and related to the potential vorticity distribution.

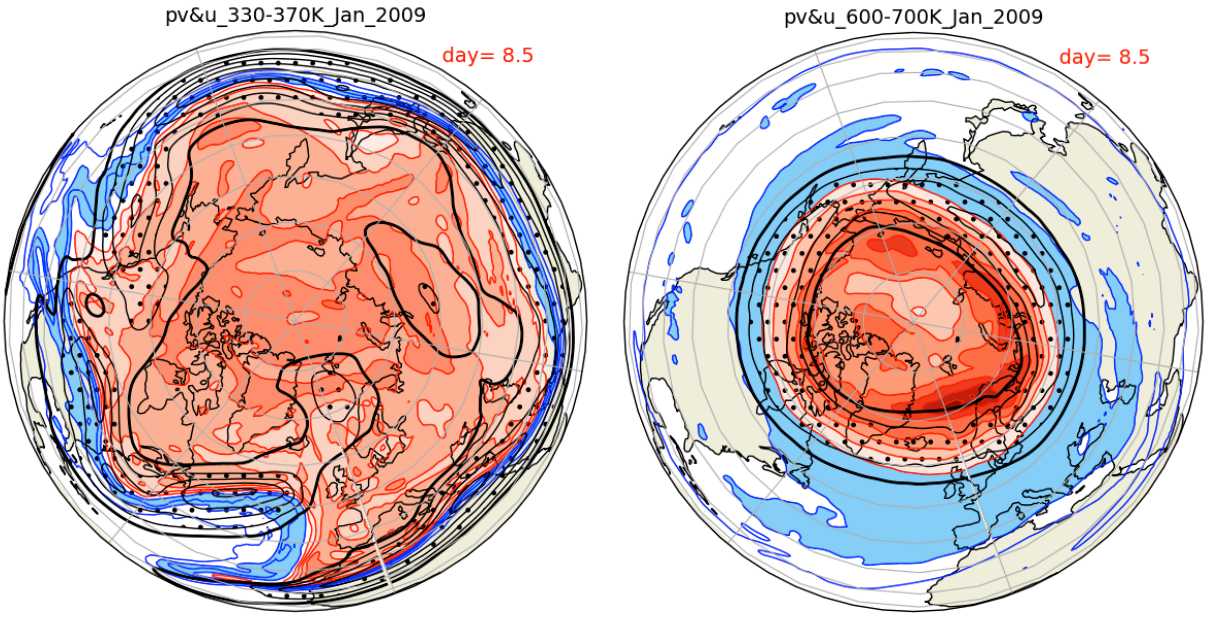

FIGURE 7.3. Potential vorticity distribution (red and blue contours and shading) and zonal (x-) component of the wind velocity (black contours and hatching) in the layer between the isentropic surfaces at 330 K and at 370 K (left) and in the layer between the isentropic surfaces at 600 K and at 700 K on January 8, 2009, 12 UTC over the Northern Hemisphere. Left panel: PV-contour interval is 1 PVU, starting at 1 PVU (blue). First red PV-contour at 5 PVU. Right panel: PV-contour interval is 40 PVU, starting at 40 PVU (blue). First red PV-contour at 120 PVU. Both panels: contour-interval wind velocity (black) is 10 m s^{-1}; first contour at 20 m s^{-1}; hatching if u>30 m s^{-1}. Based on the ERA-Interim reanalysis (https://apps.ecmwf.int).

7.2 Potential vorticity inversion equation

Potential vorticity inversion is based on the assumption that the atmosphere is both in gradient wind balance and in hydrostatic balance. This assumption is applied here to the "primary" circulation, i.e. to the simplified situation of a circumpolar zonal (west-east) flow that is axisymmetric about the pole. In other, words, we can restrict out attention to **zonal mean quantities, which are indicated here by square brackets**, i.e. $[u]$ is the zonal mean of u.

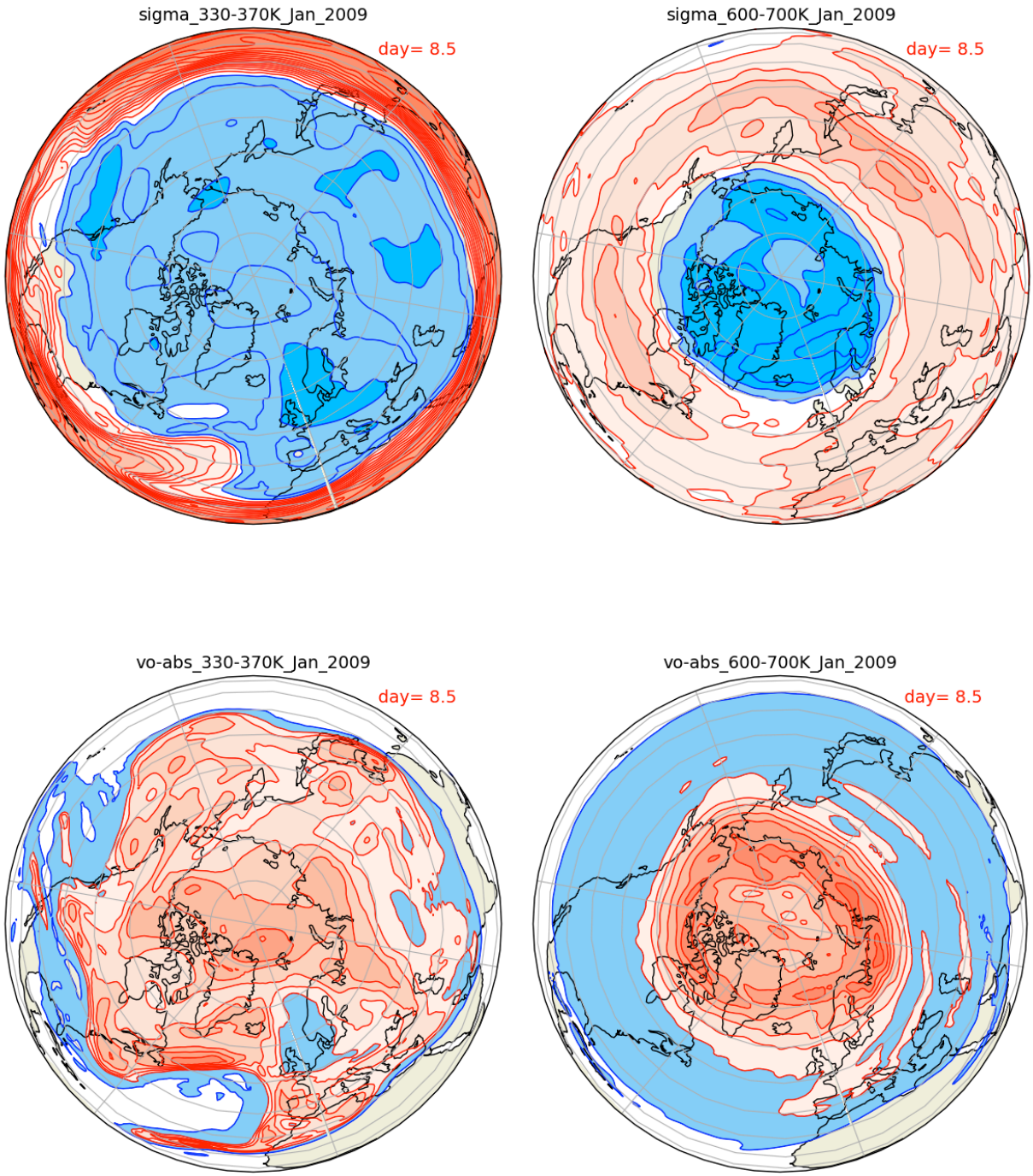

FIGURE 7.4. Upper panels: Isentropic density, σ (eq. 9, **Box 7.1**) in the layer 330-370 K (left) and in the layer 600-700 K (right) on January 8, 2009, 12 UTC. Lower panels: absolute vorticity, $(\zeta_\theta + f)$ in the layer 330-370 K (left) and in the layer 600-700 K (right) on January 8, 2009, 12 UTC. Left-upper panel: σ -contour interval is 5 kg m^{-2} K^{-1}, starting at 5 kg m^{-2} K^{-1}. Blue: σ<30 kg m^{-2} K^{-1}. Red: σ>30 kg m^{-2} K^{-1}. Right-upper panel: σ -contour interval is 0.1 kg m^{-2} K^{-1}, starting at 0.1 kg m^{-2} K^{-1}. Blue: σ<1 kg m^{-2} K^{-1}. Red: σ>1 kg m^{-2} K^{-1}. Lower panels: contour interval is 2×10^{-5} s^{-1} if $(\zeta_\theta + f)>10^{-4}$ s^{-1}. Red shading: $(\zeta_\theta + f)>10^{-4}$ s^{-1}. Blue shading: 0.5×10^{-4} s^{-1}<$(\zeta_\theta + f)<10^{-4}$ s^{-1}. Based on the ERA-Interim reanalysis (https://apps.ecmwf.int).

With potential temperature, θ, as a vertical coordinate, the balance between the zonal mean pressure gradient, the zonal mean Coriolis force and the zonal mean centrifugal force is (compare with eq. 3 of **Box 7.1**).

$$\boxed{\frac{[u]^2 \tan\phi}{a} = -\frac{\partial[\Psi]}{\partial y} - f[u]} . \qquad (7.1)$$

The derivative of the streamfunction with respect to y is performed with θ constant. Hydrostatic balance in the isentropic coordinate system is written as follows (eq. 5 of **Box 7.1**):

$$\boxed{\frac{\partial[\Psi]}{\partial\theta} = [\Pi]} . \qquad (7.2)$$

Dropping the subscript, θ, in eq. 8 (**Box 7.1**), we write the definition of zonal mean **potential vorticity** as

$$[Z] = \left[\frac{\zeta + f}{\sigma}\right] \approx \frac{[\zeta] + f}{[\sigma]} . \qquad (7.3)$$

The zonal mean of **relative vorticity** is

$$[\zeta] = \frac{[u]\tan\phi}{a} - \frac{\partial[u]}{\partial y} , \qquad (7.4)$$

and the zonal mean of **isentropic density** is

$$[\sigma] = -\frac{1}{g}\frac{\partial[p]}{\partial\theta} . \qquad (7.5)$$

Differentiating (7.3) with respect to y and using (7.5) yields (assuming g constant)

$$[\sigma]\frac{\partial[Z]}{\partial y} = \frac{\partial[\zeta]}{\partial y} + \frac{[Z]}{g}\frac{\partial}{\partial\theta}\left(\frac{\partial[p]}{\partial y}\right) + \frac{\partial f}{\partial y} . \qquad (7.6)$$

From gradient wind balance (7.1) and hydrotatic balance (7.2) the following equation for **thermal wind balance** is obtained:

$$f_{loc}\frac{\partial[u]}{\partial\theta} = -\frac{\partial[\Pi]}{\partial y} . \qquad (7.7)$$

In (7.7)

$$\boxed{f_{loc} = f + \frac{2[u]\tan\phi}{a}} . \qquad (7.8)$$

Using the definition of the Exner function (eq. 6, **Box 7.1**),

$$\Pi = c_p\left(\frac{p}{p_{ref}}\right)^{\kappa} \quad , \tag{7.9}$$

and the ideal gas law ($p=R\rho T$, ρ being density), the right hand side of (7.7) can be rewritten as follows:

$$\frac{\partial[\Pi]}{\partial y} = \frac{1}{\theta[\rho]}\frac{\partial[p]}{\partial y} \quad , \tag{7.10}$$

so that eq. 7.7 becomes

$$f_{loc}\theta[\rho]\frac{\partial[u]}{\partial\theta} = -\frac{\partial[p]}{\partial y} \quad . \tag{7.11}$$

Using (7.4) and (7.11), (7.6) becomes

$$\boxed{\frac{\partial}{\partial y}\left(\frac{\partial[u]}{\partial y} - \frac{[u]\tan\phi}{a}\right) + \frac{[Z]}{g}\frac{\partial}{\partial\theta}\left(f_{loc}\theta[\rho]\frac{\partial[u]}{\partial\theta}\right) = \frac{df}{dy} - [\sigma]\frac{\partial[Z]}{\partial y}} \tag{7.12}$$

This equation, which **is in fact a formulation of thermal wind balance in terms of potential vorticity**, is also a version of the equation expressing the **principle of invertibility of potential vorticity**[4]. It describes the balanced response, in terms of the zonal average zonal flow, $[u]$, to a specified zonally symmetric distribution of the potential vorticity $[Z]$. If $f_{loc}[Z]>0$, eq. 7.12 is an **elliptic non-linear partial differential equation** (**Box 7.2**). Finding the solution, $[u(y,\theta)]$, given $[Z(y,\theta)]$, is complicated by the nonlinearity of the equation and by the inhomogeneous lower boundary condition. The following sections describe in detail how the solution of (7.12) is obtained, including the complications resulting from imposing the boundary conditions.

Equation 7.12 seems to be a rather complicated way of formulating thermal wind balance. The potential vorticity is not a variable that is directly measured, although it can be deduced from measurements of temperature, pressure and wind velocity. So, why do we want to have an equation for the wind velocity in terms potential vorticity? What makes equation 7.12 so attractive, despite its great complexity?

The answer to this question is the following. Because potential vorticity is conserved in adiabatic conditions, the full PV-evolution equation (eq. 11, **Box 7.1**), which is repeated here:

$$\boxed{\frac{dZ_\theta}{dt} = Z_\theta\frac{\partial}{\partial\theta}\frac{d\theta}{dt} + \frac{1}{\sigma}\frac{\partial u}{\partial\theta}\frac{\partial}{\partial y}\frac{d\theta}{dt} - \frac{1}{\sigma}\frac{\partial v}{\partial\theta}\frac{\partial}{\partial x}\frac{d\theta}{dt} + \frac{1}{\sigma}\left(\frac{\partial F_y}{\partial x} - \frac{\partial F_x}{\partial y}\right)}, \tag{7.13}$$

[4] Equation 7.12 is analogous to eq. 29 of Hoskins et al. (1985) (list of articles at the end of this section)

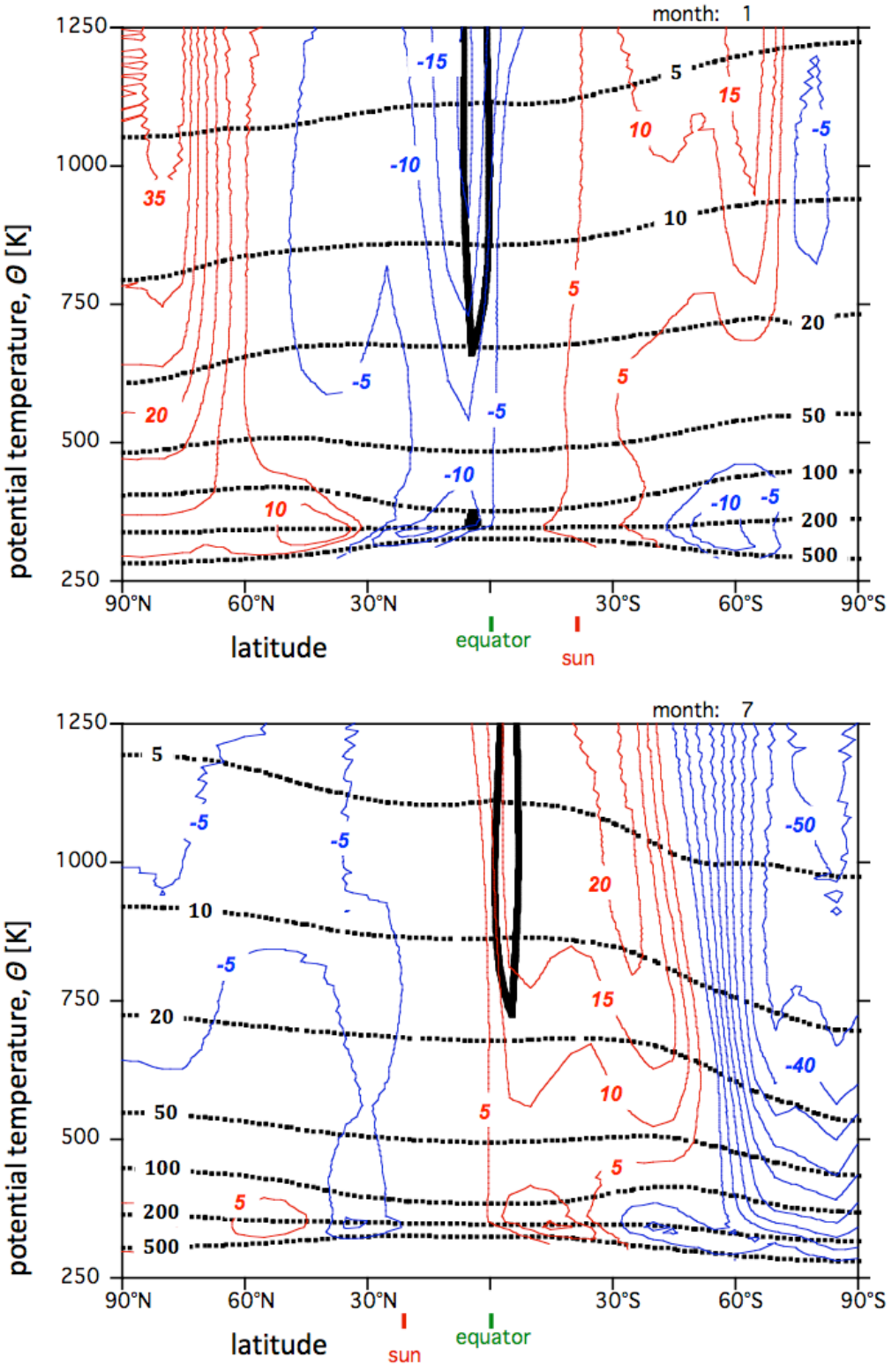

FIGURE 7.5. The zonally averaged, monthly average pressure and relative vorticity (eq. 7.54) according to the CIRA (**Table 1.1**), as a function of latitude and potential temperature. Relative vorticity is labeled in units of 10^{-6} s^{-1} (red contours: postive values; blue contours: negative values). The dashed lines are isobars labeled in hPa. The black thick solid line marks the boundary of the narrow band on the winter side of the equator where $f_{loc}Z<0$, i.e. where the zonally averaged state is **inertially unstable**. Upper panel: January; lower panel: July.

is attractive as a single differential equation that governs the dynamical evolution of the atmosphere, because material potential vorticity changes can be attributed fully to diabatic effects. Furthermore, given potential vorticity, and assuming that the atmosphere remains very close to thermal wind balance, the PV-inversion equation relates potential vorticity to all the other thermodynamic variables (temperature, pressure and wind), because its solution yields the wind velocity and the associated pressure and temperature through the balance requirements. Therefore, the behaviour of the atmosphere can be understood from only two equations (eqs. 7.12 and 7.13), given knowledge of boundary conditions and diabatic effects.

If $f_{loc}Z<0$, eq. 7.12 is **not elliptic and, therefore, does not have a unique solution**. The criterion $f_{loc}Z<0$ corresponds to the criterion for **inertial instability** on an isentropic surface. A region of inertial instability is usually found within 10° of the equator on the winter hemisphere side of the equator (**figure 7.5**), epecially in the months December to February (in the northern hemisphere winter) and June to August (in the southern hemisphere winter). Inertial instability or weak inertial stability, presumably, is the reason for the **relatively intense winter cross-equatorial Hadley cell** (**chapter 12**).

Box 7.2 Elliptic partial differential equations

In fluid dynamics elliptic partial differential equations arise in problems where some form of equilibrium is imposed, such as thermal wind balance (eq. 7.7) in the case of eq. 7.12. We'll encounter more partial differential equations of the elliptic type, such as the "omega equation" in **section 1.43** and the Kuo-Eliassen equation in **section 11.5**.

The prototype second-order partial differential equation with two independent variables is

$$A(x,y)\frac{\partial^2 u}{\partial y^2}+2B(x,y)\frac{\partial^2 u}{\partial y\partial x}+C(x,y)\frac{\partial^2 u}{\partial x^2}=f\left(x,y,u,\frac{\partial u}{\partial y},\frac{\partial u}{\partial x}\right) \qquad (1)$$

This equation is of the elliptic type if

$$B^2-4AC<0$$

Eq. 7.12, thus, is of the elliptic type if $f_{loc}Z_\theta>0$. The function f can be written as

$$f\left(x,y,u,\frac{\partial u}{\partial x},\frac{\partial u}{\partial y}\right)=D(x,y)\frac{\partial u}{\partial x}+E(x,y)\frac{\partial u}{\partial y}+F(x,y)u+G(x,y)$$

If eq. 1 is elliptic this equation possesses one and only one solution in a given region, bounded by a *smooth* curve with $u=H(x,y)$ on this curve and provided that in this region (including the boundary)

(i) A, B, and C are continuously differentiable,
(ii) D, E, F, G and H are continuous,

In the case of eq. 7.12, $A=1$, $B=0$, $D=-(\tan(\phi)/a)$, $F=-(a\cos(\phi))^{-2}$ and $G=\mathrm{d}f/\mathrm{d}y-\sigma\partial Z/\partial y$. So, A and B are continuously differentiable and D, F and G are continuous. However, because f_{loc}

depends on u, the functions C and E also depend on u, implying that eq. 7.12 is a non-linear version of the prototype elliptic partial differential equation (1). In particular, when we apply the chain rule to the second term on the l.h.s. of eq. 7.12, we encounter a term containing a factor $(\partial u/\partial\theta)^2$ which does not fit in with this prototype equation (see eq. 7.8).

In the vicinity of the equator eq. 7.12 is very likely not elliptic. In January, for example (**figure 7.5**), $f_{\rm loc}Z<0$ equatorward of 10°N. The southern boundary of the domain of solution of eq. 7.12 should therefore lie north of this latitude. Physically speaking, the condition, $f_{\rm loc}Z<0$, is associated with the (inertial) instability of thermal wind balance (**section 1.19**).

The standard formulation of the boundary condition for the solutions of an elliptic second order partial differential equation is to specify u on the boundary (*Dirichlet boundary condition*) or to specify the normal derivative of u on the boundary (*Neumann boundary condition*). In the problem at hand, we impose a Dirichlet boundary condion at the pole, at the upper boundary and at 10°N. At the lower boundary, which is not a smooth curve, we impose a numerical approximation of the Neumann boundary condition by prescribing $\partial u/\partial\theta$.

Therefore, because of the non-linearity of eq. 7.12 and because of the complexity of formulating a boundary condition, the solution of this equation is far from a standard mathematical problem.

7.3 Reference state and the character of zonal mean PV-anomalies

At first glance, the zonal mean potential vorticity distribution, shown in **figure 7.1**, demonstrates little relation with the zonal mean zonal wind distribution. In particular, it is almost impossible to identify the jets with particular features in the potential vorticity distribution. The PV-inversion equation (7.12), nevertheless, states that such a relation exists. It is the intention of this section to identify that part of the **PV-distribution that is "inducing" the zonal mean zonal flow**.

Zonal mean potential vorticity, zonal mean isentropic density and zonal mean relative vorticity can be partitioned into a **reference state**, indicated by the subscript 'ref', and an **anomaly**, indicated by a prime, as follows.

$$[Z] = Z_{\rm ref} + Z' \; ; \tag{7.14a}$$

$$[\sigma] = \sigma_{\rm ref} + \sigma' ; \tag{7.14b}$$

$$[\zeta] = \zeta_{\rm ref} + \zeta' \; . \tag{7.14c}$$

The reference isentropic density is determined by horizontally averaging the isentropic density over the domain of interest. Since we are restricting our attention here to the case where σ is a function only of latitude, ϕ, and potential temperature, θ, this becomes

$$\boxed{\sigma_{\rm ref} = \frac{\int \sigma \cos\phi d\phi}{\int \cos\phi d\phi}} \; . \tag{7.15}$$

Here, the integral in (7.15) is over the northern hemisphere from 10°N to the North Pole. As was stated before, the equatorial region is excluded because of the occurrence of inertial instability (**figure 7.5**), making thermal wind balance impossible. The reference potential vorticity, $Z_{\rm ref}$, and $\sigma_{\rm ref}$ are related by,

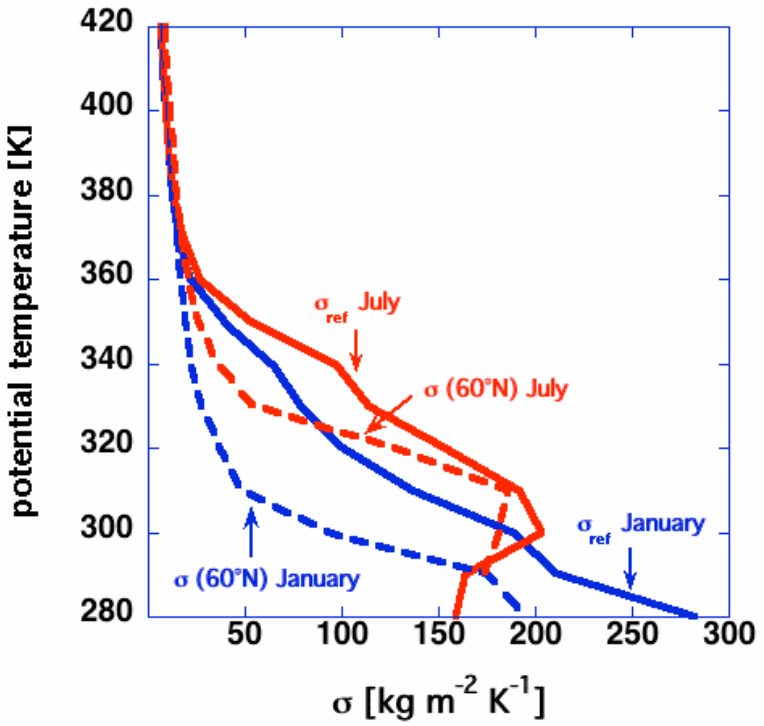

FIGURE 7.6. The average isentropic density (σ_{ref}) between 10°N and the North Pole in **January (blue solid line)** and **July (red solid line)** as a function of potential temperature, and the zonal mean isentropic density at 60°N (January average: blue dashed line; July average: red dashed line) according to the Cospar International Reference Atmosphere (**Table 1.1**).

$$\boxed{Z_{\text{ref}} = \frac{f}{\sigma_{\text{ref}}}}. \tag{7.16}$$

Because f depends on y and σ_{ref} depends on θ, Z_{ref} depends on θ *and* y. If $[\sigma]=\sigma_{\text{ref}}$ and $[Z]=Z_{\text{ref}}$ then $[\zeta]=\zeta_{\text{ref}}=0$. From the circulation theorem (**section 1.22**) and with $[u]=0$ at the pole we conclude that the **reference state corresponds to the state of rest**. This is confirmed by observing that the right hand side of eq. 7.12 is equal to zero if $Z=Z_{\text{ref}}$, i.e. the "forcing term on the r.h.s. of eq. 7.12 is equal to zero if there is no PV-anomaly. In that case the solution of eq. 7.12, with $[u]=0$ at the boundaries of the domain of interest, is $[u]=0$ in the interior of the domain.

It is easily deduced that the relation between the PV-anomaly, Z', and the associated separate vorticity- and isentropic density anomalies is given by

$$\frac{Z'}{Z_{\text{ref}}} = \frac{\zeta'}{f} - \left(1+\frac{Z'}{Z_{\text{ref}}}\right)\frac{\sigma'}{\sigma_{\text{ref}}}, \tag{7.17a}$$

or, in non-dimensional form:

$$\boxed{Z^{+} = \zeta^{+} - \left(1+Z^{+}\right)\sigma^{+}}, \tag{7.17b}$$

where

$$\boxed{Z^+ \equiv \frac{Z'}{Z_{\text{ref}}};\ \zeta^+ \equiv \frac{\zeta'}{f};\ \sigma^+ \equiv \frac{\sigma'}{\sigma_{\text{ref}}}}\ . \qquad (7.18)$$

Z^+ is referred as the "normalized PV-anomaly". According to (7.17a,b), a positive PV-anomaly will probably give rise to both a positive vorticity (cyclonic) anomaly and a negative isentropic density anomaly.

If the PV-anomaly is relatively weak, i.e. if $Z^+ << 1$, we obtain the linear approximation of (7.17a,b):

$$\boxed{Z^+ = \zeta^+ - \sigma^+}. \qquad (7.19)$$

The definition of the reference state isentropic density (i.e. σ_{ref}) is somewhat arbitrary. Nevertheless, as long as σ_{ref} depends *only* on potential temperature, the reference state is associated with the state of rest, while the anomaly is associated with, i.e. "induces", the full flow field. In this context, it might be better to refer to the "positive and negative anomalies" of Z^+ as "maxima and minima" of Z^+. However, we will stick to the former terminology, because this terminology is commonly used.

Figure 7.6 shows the monthly average value of σ_{ref} as well as of $[\sigma]$ at 60°N as a function of potential temperature for January and for July. Clearly, isentropic density is a strong function of potential temperature. Furthermore, below 360 K we observe large negative deviations from the reference value, exceeding 50% of this reference value, i.e. $\sigma^+ < -0.5$. Above 360 K these deviations are no more than about 20% of the reference value.

The reference state potential vorticity undergoes a seasonal cycle under influence of seasonal changes in the σ_{ref}. This seasonal cycle, however, does *not* induce a seasonal cycle in the circumpolar flow.

The monthly average distributions of Z_{ref}, defined in (7.16), Z^+, defined in (7.18), and pressure ($[p]$), as a function of latitude and potential temperature in the CIRA, are shown in **figure 7.7** for January and July. An interesting feature that stands out clearly, is the strong positive PV-anomaly, with values of Z^+ exceeding 2 non-dimensional units in both months at levels between 200 hPa and 400 hPa. This PV-anomaly, which is present year round in both hemispheres, appears to coincide approximately with the Z_{ref}=2 PVU isopleth, which is called "**the reference dynamical tropopause**". Following the terminology of Gettelman et al. (2011)[5], we refer to this PV-anomaly as the "**extra-tropical UTLS PV-anomaly**" ("UTLS" stands for "Upper Troposphere/Lower Stratosphere"), in short: "**ex-UTLS PV-anomaly**". Note that the isopleths of pressure (the black dotted lines in **figure 7.7**) in the layer between 320 and 380 K are squeezed together in the tropics, indicating that this layer contains more mass in the tropics than in the mid-latitudes. The ex-UTLS PV-anomaly, indeed, is manifest principally as a mass anomaly, or isentropic density anomaly. This is seen more clearly in **figure 7.10**, which will be discussed later.

In the winter hemisphere (January in the northern hemisphere and July in the southern hemisphere) we identify a positive PV-anomaly in the stratosphere above about 500 K. This PV-anomaly extends to much greater heights than is shown here. The stratospheric PV-anomaly exhibits a strong seasonal cycle, giving way to a negative PV-anomaly in summer.

---

[5] Gettelman, A., P. Hoor, L.L.Pan, W.J. Randel, M.I. Hegglin, T. Birner: 2011: The extratropical upper troposphere and lower stratosphere. **Rev.Geophys.**, **49**, RG3003, doi:10.1029/2011RG000355.

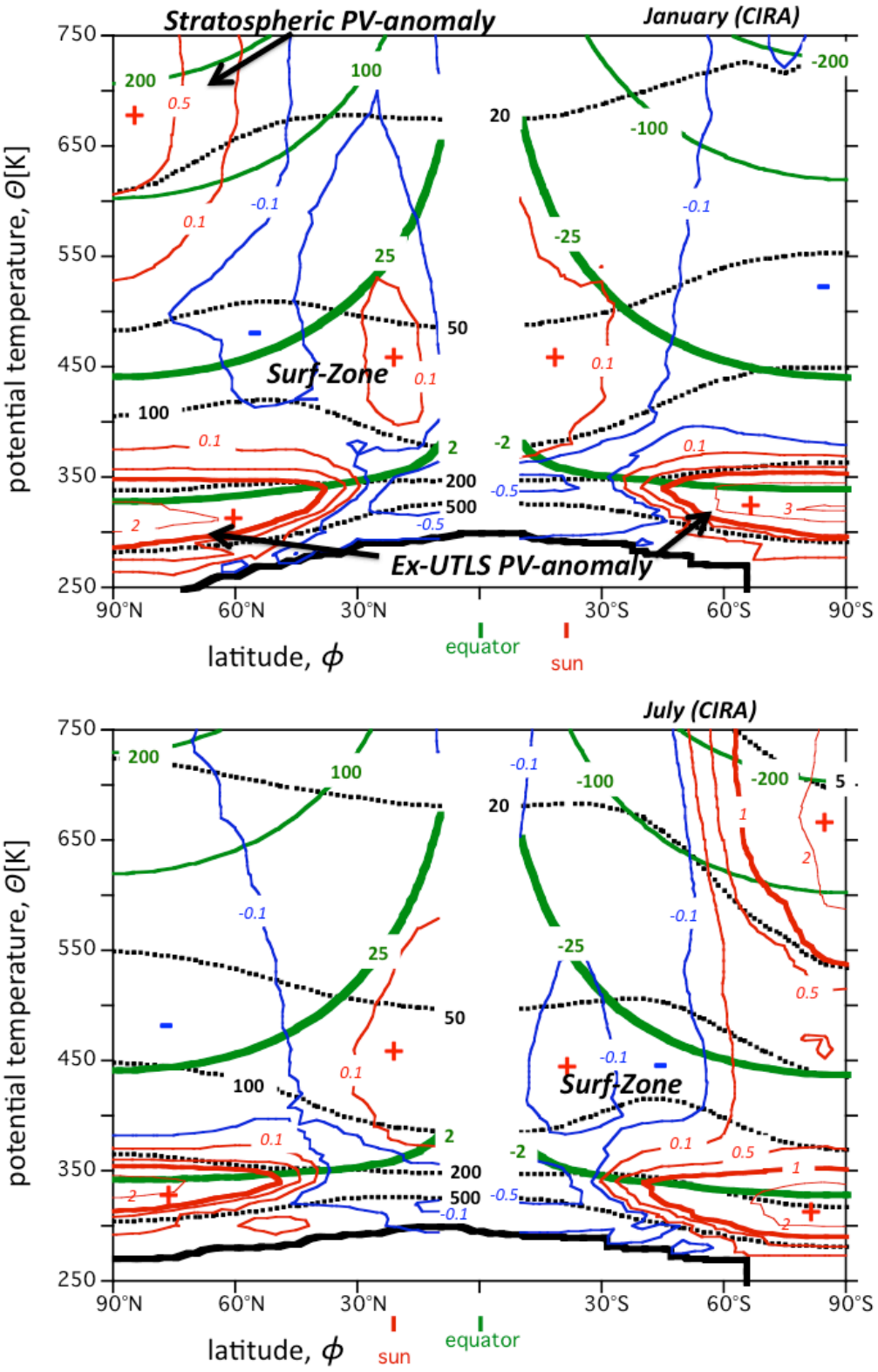

FIGURE 7.7. The zonal average distributions of Z_{ref} (green contours; labeled in PVU), Z^+ (red: positive; blue: negative; labeled in non-dimensional units) and pressure (dotted; labeled in hPa) as a function of latitude and potential temperature for January and July. Plus- and minus signs indicate maxima and minima in Z^+, respectively. Contours within 10° of the equator are not drawn. The thick black line corresponds to the Earth's surface. The contours of Z^+ correspond to the values, ±0.1, ±0.5,±1, ±2 and ±3 units. The line corresponding to Z_{ref}=2 PVU is the "**reference dynamical tropopause**". The **surf-zone** is characterised by a reversed isentropic gradient of Z^+. Analysis based on the COSPAR International Reference Atmosphere (Fleming et al., 1990).

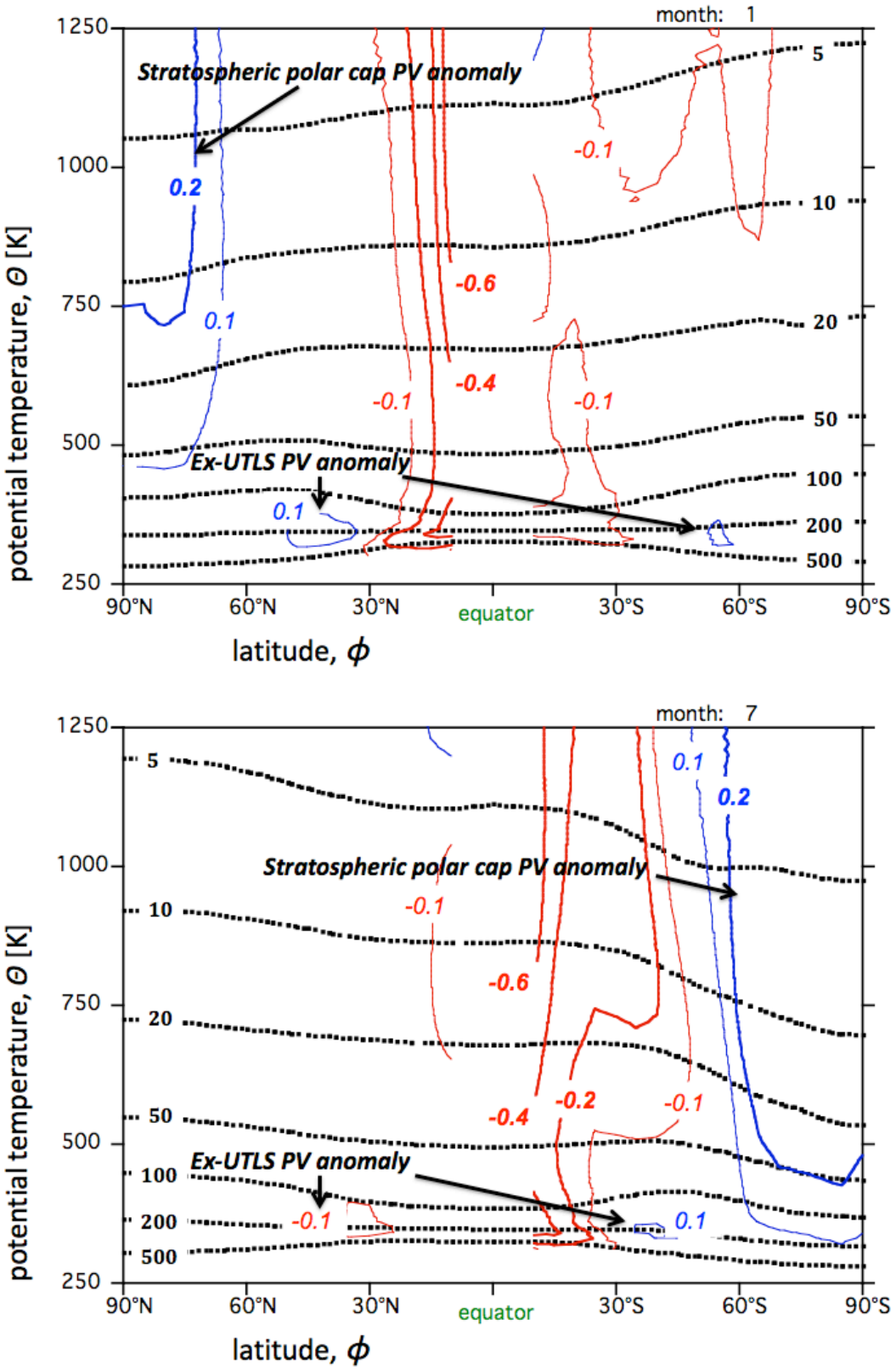

FIGURE 7.8. The CIRA (**Table 1.1**) monthly mean, zonal mean normalized relative vorticity anomaly, ζ^+ (defined in eq. 7.18) in January (upper panel) and in July (lower panel), labeled in non-dimensional units. Also shown is the pressure field (dashed lines, labeled in hPa). The positive stratospheric polar cap PV-anomaly in the winter hemisphere is manifest more strongly as a vorticity anomaly than the Ex-UTLS PV-anomaly.

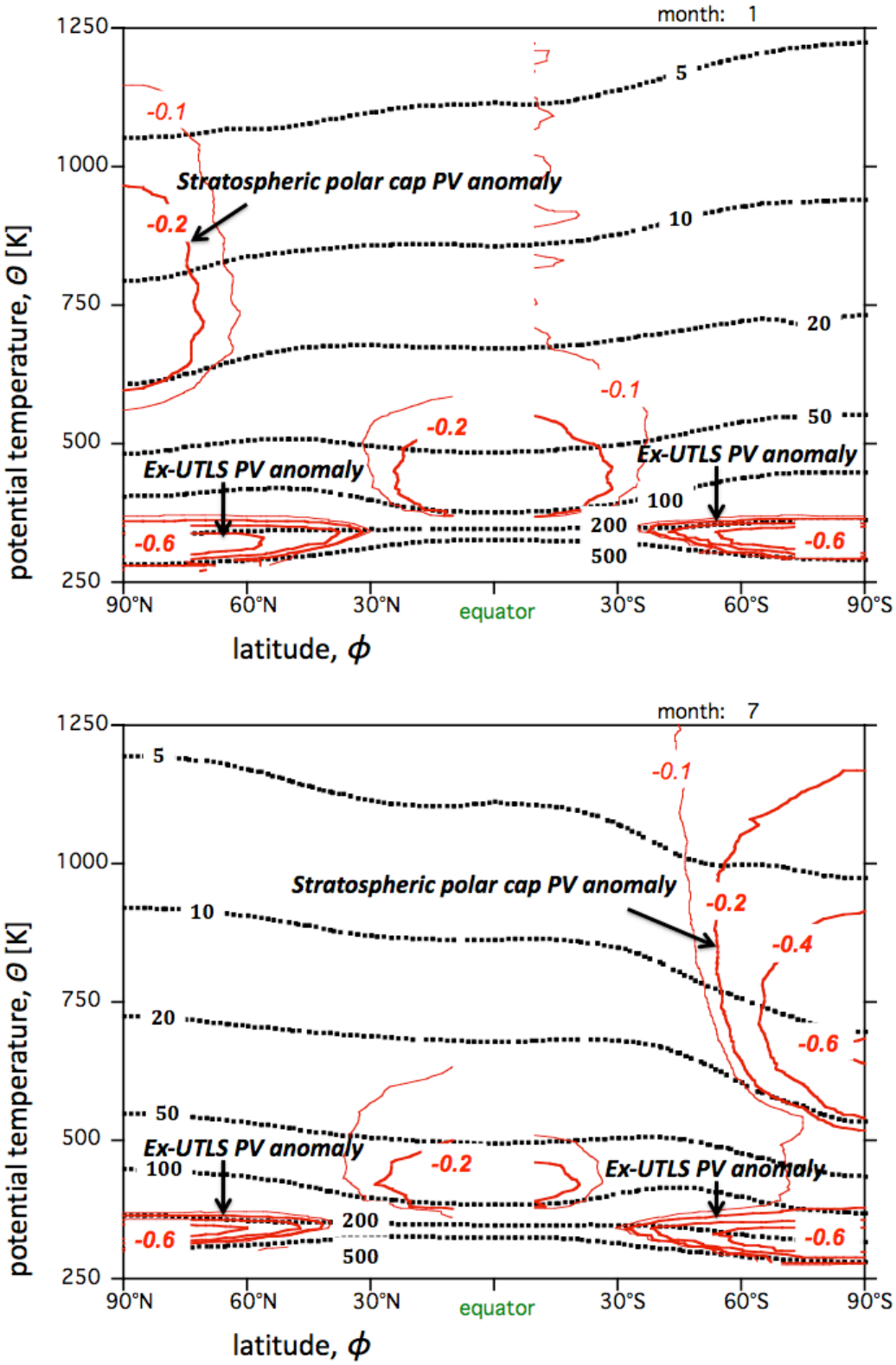

FIGURE 7.9. The CIRA (**Table 1.1**) monthly mean, zonal mean normalized isentropic density anomaly, σ^+ (defined in eq. 7.18) in January (upper panel) and in July (lower panel), labeled in non-dimensional units, where only negative anomalies are shown. Also shown is the pressure field (dashed lines, labeled in hPa). The positive ex-UTLS PV-anomaly is manifest very strongly as a negative mass anomaly. The stratospheric polar cap PV-anomaly in the winter hemisphere is manifest more strongly as a negative mass anomaly in the southern hemisphere than in the northern hemisphere.

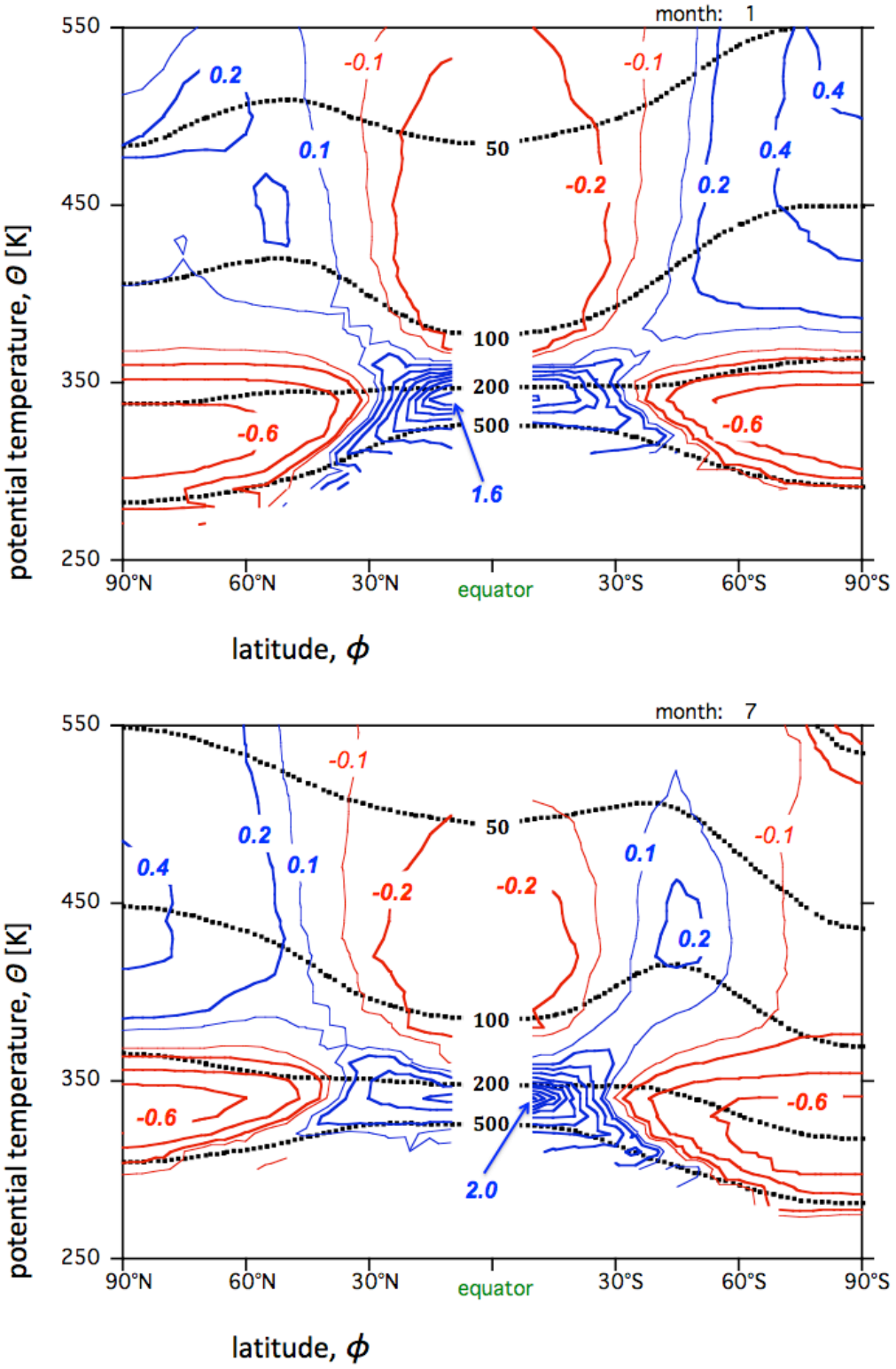

FIGURE 7.10. Close-up view of the lower part of the previous figure, where positive anomalies are also shown, i.e. the monthly mean, zonal mean normalized isentropic density anomaly, σ^* in January (upper panel) and in July (lower panel), labeled in non-dimensional units. Also shown is the pressure field (dashed lines, labeled in hPa). The positive Ex-UTLS PV anomalies in both summer and winter hemispheres are formed due to the opposite effects on potential vorticity of diabatic upwelling ($d\theta/dt>0$) between 290 K and 380 K in the tropics and diabatic downwelling ($d\theta/dt<0$) in the extra-tropics between the same levels (chapter 12). The formation-mechanisms of these anomalies are addressed in detail in chapter 12 (see also section 7.14).

In the ex-UTLS PV-anomaly $|Z^+|>1$, while higher up in the stratosphere $|Z^+|$ is usually much smaller than 1, the only exception being winter stratosphere above 550 K in the southern hemisphere where $|Z^+|$ exceeds a value of 2. This translates into an intense southerm hemisphere polar winter stratospheric jet.

The PV-distribution equatorward of 10° latitude is not shown because, as was stated before, the reference isentropic density is determined by averaging poleward of 10° latitude for each hemisphere separately, using eq. 7.15. For the monthly average distribution of potential vorticity in the two months shown in **figure 7.7** (January and July), the criterion for inertial stability is fulfilled everywhere in both hemispheres, pole-ward of 10° latitude (**figure 7.5**).

Figure 7.8 shows ζ^+ while **figure 7.9** shows σ^+ as a function of latitude and potential temperature in January and July. We observe that the ex-UTLS PV-anomaly is manifest strongly as an isentropic density- (or mass-) anomaly. Eq. 7.17b demonstrates that two factors contribute to the amplitude of the PV-anomaly. In the case of the ex-UTLS PV-anomaly, the second term on the r.h.s. of eq. 7.17b is more than an order of magnitude larger than the first term. Therefore, the ex-UTLS PV-anomaly is almost completely determined by the isentropic density anomaly. **Figure 7.10** gives a more detailed picture of the isentropic density anomaly in the UTLS. Isentropic density anomalies are negative in the extratropics and positive in the tropics. The stratospheric PV anomaly is about equally manifest as a relative vorticity anomaly and as a isentropic density anomaly.

The difference in the character of the two positive PV-anomalies is the result of two principal "diabatic mechanisms" that lead to a local change in potential vorticity. The first mechanism is the "diabatic stretching mechanism" (the first rem on the r.h.s. of eq. 7.13). The second "mechanism" is the result of "advection of PV" due to cross-isentropic flow. The "tilting terms" on the r.h.s. of eq. 7.13 are less important. Neglecting these terms and also neglecting the frictional terms, the PV-equation can be written as follows:

$$\frac{\partial Z_\theta}{\partial t} + u\left(\frac{\partial Z_\theta}{\partial x}\right)_\theta + v\left(\frac{\partial Z_\theta}{\partial y}\right)_\theta = -\frac{d\theta}{dt}\frac{\partial Z_\theta}{\partial \theta} + Z_\theta \frac{\partial}{\partial \theta}\frac{d\theta}{dt}. \qquad (7.20)$$

Due to the strong positive vertical PV-gradient in the stratosphere and the diabatic cooling over the winter pole in the stratosphere, the **first** term on the r.h.s., i.e. the diabatic advection term, dominates in the middle to upper polar winter stratosphere . The second term on the r.h.s., i.e. the "stretching term", is most important in the tropical troposphere and lower stratosphere, due to strong vertical gradients in latent heating. More details on this question are given in chapter 12.

7.4 Scale of the "response" to a PV-anomaly

In this section we solve a strongly simplified version of the PV-inversion eq. 7.12. From this solution we identify a fundamental spatial scale relation that governs adjustment to thermal wind balance.

We first assume that

$$\frac{u\tan\phi}{a} << \frac{\partial u}{\partial y}, f_{\text{loc}} \approx f_{\text{ref}} = \text{constant}, \rho f_{\text{ref}}\theta = \text{constant}, \sigma_{\text{ref}} = \text{constant}.$$

Here, f_{ref} is the area weighted average of f over the northern hemisphere. We obtain a highly simplified (linearised) version of eq. 7.12:

$$\frac{\partial^2[u]}{\partial y^2} + A\frac{\partial^2[u]}{\partial \theta^2} = -\sigma_{\text{ref}}\frac{\partial Z'}{\partial y}, \tag{7.21}$$

where

$$A \approx \frac{f_{\text{ref}}\theta Z_{\text{ref}}[\rho]}{g} \approx \text{constant}. \tag{7.22}$$

By applying the method of "separation of varables", we assume that $u(y,\theta)$ and $Z'(y,\theta)$ depend on y and θ according to

$$[u] = \mathrm{U}(\theta)\sin\frac{2\pi(y_{NP}-y)}{L};\ Z' = \mathrm{Z}(\theta)\cos\frac{2\pi(y_{NP}-y)}{L}. \tag{7.23}$$

The parameter, y_{NP}, is the distance from the equator to the North Pole. **The horizontal scale of both the "response" (the zonal wind, $[u]$) and the "forcing" (the potential vorticity anomaly, centred at the North Pole) is proportional to L**. This is so, because the equation (7.21) governing the "response", is linear. We take this solution seriously (physically) only for $|y_{NP}-y|<L/2$. Substituting (7.23) into (7.21) yields,

$$\frac{\partial^2 \mathrm{U}}{\partial\theta^2} - \frac{4\pi^2}{AL^2}\mathrm{U} = -\frac{2\pi\sigma_{\text{ref}}}{AL}\mathrm{Z}. \tag{7.24}$$

This is an inhomogeneous "Helmholtz equation".

We now assume that the potential vorticity anomaly is located at a certain (*discrete*) height or potential temperature, θ_0. For $\theta\neq\theta_0$, the right hand side of eq. 7.24 is equal to zero. Therefore, here eq. 7.24 is a homogeneous differential equation with the following solution.

$$\mathrm{U} = C_1\exp\left(\frac{2\pi(\theta-\theta_0)}{L\sqrt{A}}\right) + C_2\exp\left(-\frac{2\pi(\theta-\theta_0)}{L\sqrt{A}}\right), \tag{7.25}$$

where C_1 and C_2 are constants determined by the boundary conditions. Assume, for simplicity, that the boundaries are located very far away from the potential vorticity anomaly and that U goes to zero at these boundaries. If $A>0$ (which is the case if $Z_{ref}>0$, which is practically always the case in the northern hemisphere), this implies that

$$\mathrm{U} = C\exp\left(-\frac{2\pi|\theta-\theta_0|}{L\sqrt{A}}\right), \tag{7.26}$$

where C is a constant, which is determined by the "boundary condition" at $\theta=\theta_0$. The solution, therefore, describes an exponentially decaying function of θ with a maximum or minimum value at the discrete level $\theta=\theta_0$ where Z is non-zero (**figure 7.11**).

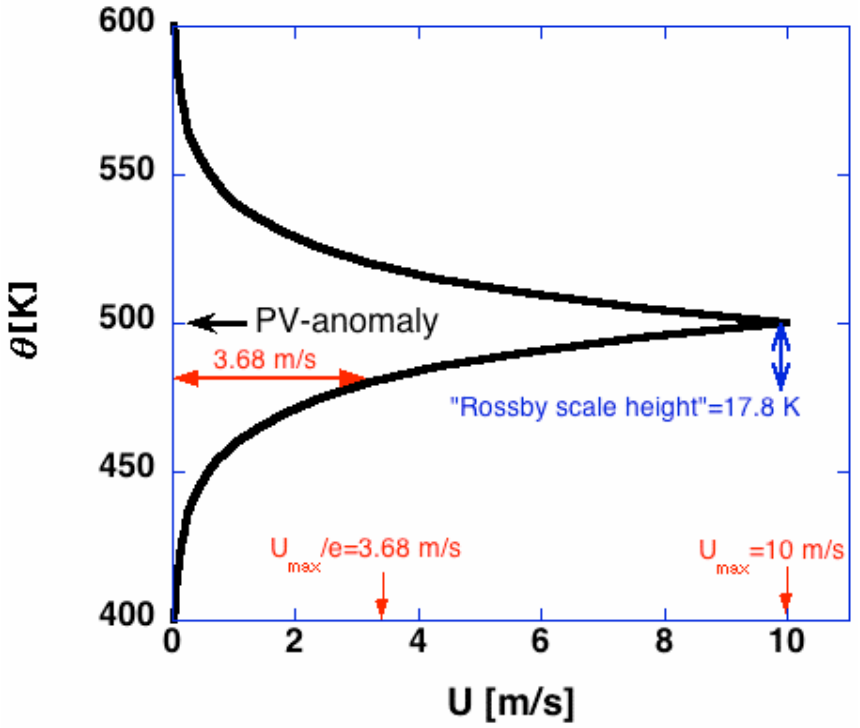

FIGURE 7.11. The amplitude of the azimuthal wind as a function of potential temperature, induced by a hypothetical PV-anomaly at a discrete level $\theta=\theta_0=500$K. The parameter values that were used to draw this graph have the following values: L=500 km, $A=5\times10^{-8}$ K m^{-2} and C=10 m/s. The Rossby scale "height" is explained in the text.

If $A>0$, $\partial^2 U/\partial\theta^2$ has the same sign as U for $\theta\neq\theta_0$. In order to make the solution for $\theta\neq\theta_0$ match the solution for $\theta=\theta_0$, U>0 if Z>0 and U<0 if Z<0. Therefore, in agreement with (7.17b), a **positive potential vorticity anomaly is associated with a cyclonic circulation while a negative potential vorticity anomaly is associated with an anticyclonic circulation**.

The idea, which is distilled from this semi-qualitative solution of the linearised PV-inversion equation, is that a potential vorticity anomaly induces a wind field, $[u](y, \theta)$, with a vertical dependence given approximately by eq. 7.26 (**figure 7.11**). In other words, a change in the wind field can be attributed to a change in the potential vorticity field. Alan Thorpe[6] coined the term **attribution** as a slightly weaker form of "**cause-and-effect**" to characterise the relation between potential vorticity and the induced wind field. Stated differently, **changes of the potential vorticity (due to for example heating/cooling or advection; eq. 7.20) must be accompanied by changes in the wind, in order to preserve thermal wind balance**.

The associated vertical scale, $\Delta\theta$, of the response in $[u]$ is easily distilled from eq. 7.26:

$$\Delta\theta = \frac{L\sqrt{A}}{2\pi} \,. \qquad (7.27)$$

---

[6] Thorpe, A.J., 1997: Attribution and its application to mesoscale structure associated with tropopause folds. **Q.J.R.Meteorol.Soc**.,. 123, 2377-2399.

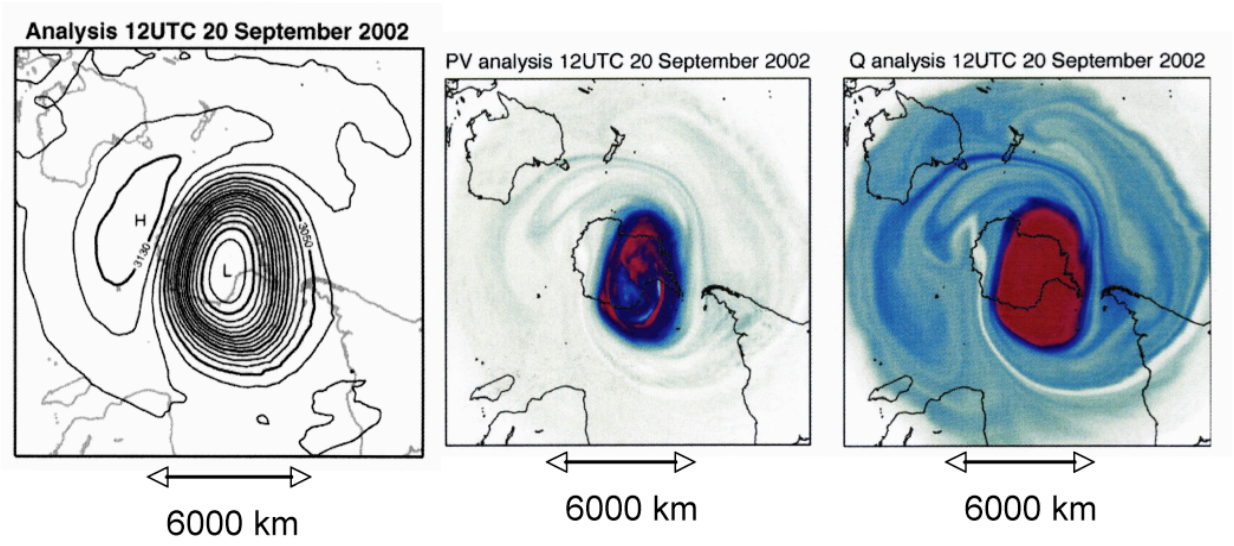

FIGURE 7.12. A PV-anomaly over the South Pole. Polar night stratospheric vortex at 10 hPa over Antarctica (September 20, 2002, 1200 UTC). Left: height (labeled in dm); middle: potential vorticity on the 850 K isentropic surface shading from 0 PVU to -1000 PVU (red); right: specific humidity on the 850 K isentropic surface shading from 2 to 3.8 (red) mg/kg. From Simons, A., M. Hortal, G. Kelly, A. McNally, A. Untach and S. Uppala, 2003: **ERA-40 project report nr 5** (ECMWF). A whole issue of Journal of the Atmospheric Sciences is devoted the the splitting of the polar vortex over the South Pole in September 2002 (**J.Atmos.Sci**. number 3, vol. 62 (2005)), an event that had not been observed before.

$\Delta\theta$ is referred to by Hoskins et al. (1985)[7] as the **"Rossby scale height"** (shortly: "Rossby height"). It measures the vertical penetration (in K) of the flow structure above and below the location of the potential vorticity anomaly, which is induced by thermal wind adjustment to this anomaly. The concept of Rossby "height" is analogous to that of the deformation scale height for hydrostatic adjustment (chapter 3) or that of the Rossby radius of deformation for geostrophic adjustment (chapter 5). Stated shortly, we may say that **a potential vorticity perturbation induces a perturbation in the wind field with a characteristic vertical scale in the order of the Rossby height.**

Tranformation of the expression for Rossby "height" (7.27) to "physical space", reveals deeper implications of the solution to the PV-inversion equation. Using hydrostatic balance, expressed as $\Delta p = -\rho g \Delta z$, and the definition of isentropic density, expressed as $\sigma = -\Delta p/(g\Delta\theta)$, eq. 7.27 becomes

$$\boxed{\frac{\Delta z}{L} = \frac{F}{2\pi N}}, \qquad (7.28)$$

where N is the buoyancy frequency, defined as (**section 1.5**),

$$N = \sqrt{\frac{g}{\theta}\frac{\Delta\theta}{\Delta z}}\ . \qquad (7.29)$$

and

[7] Hoskins, B.J., M.E. McIntyre and A.W. Robertson, 1985: On the use and significance of isentropic potential vorticity maps. **Quart.J.R.Met.Soc., 111**, 877-946. (see p. 902)

$$F \equiv \sqrt{f\left(f+\zeta_\theta\right)} \ . \qquad (7.30)$$

is the inertial frequency (**sections 1.18** and **1.20**).

Equation (7.28) is written in terms of the **aspect ratio**, $(L/\Delta z)$, of the circulation induced by a PV-anomaly. Average tropospheric conditions yield a **Rossby ratio**, $N/F \approx 10^{-2}/10^{-4}=100$ [8]. Therefore, **balanced circulation systems typically have an aspect ratio, $L/\Delta z$, of 100, i.e. they are very "flat"**. An interesting exception is the core of an intense tropical cyclone, where the magnitude of the relative vorticity can be 100 times the planetary vorticity (i.e. $\zeta_a \approx 100f$; problem 1.17; **figure 7.13** [9]), so that $F \approx 10f$, and therefore $L/\Delta z \approx 10$. Therefore, tropical cyclones have a relatively small horizontal dimension, which translates into a radius of maximum wind in the order of 100 km, or less in the case of a mature tropical cyclone. The horizontal dimension of a midlatitude cyclone, where relative vorticity usually does not significantly exceed planetary vorticity, is one order of magnitude larger (chapter 9).

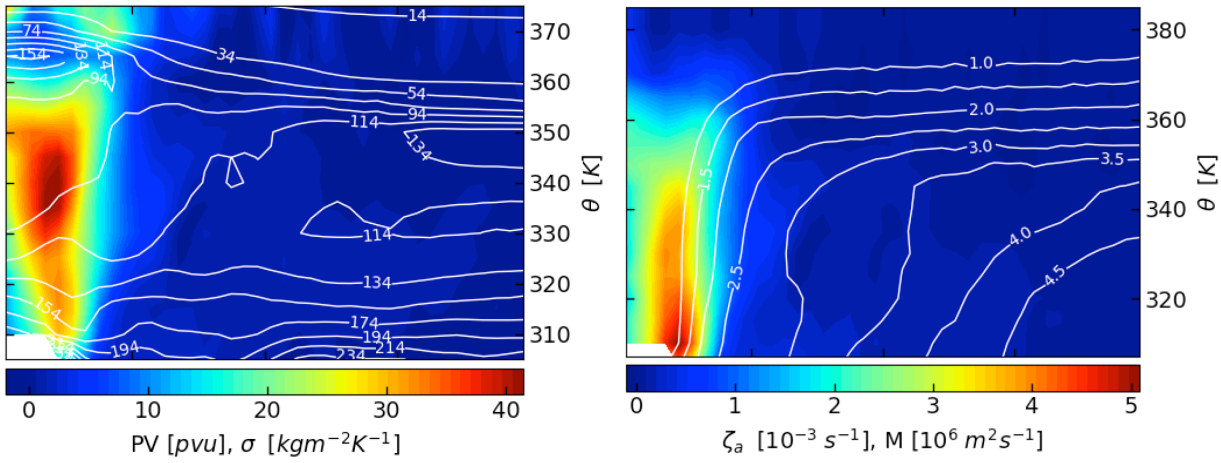

FIGURE 7.13. Vertical cross-sections of (azimuthally averaged) PV and isentropic density (contours labeled in kg $m^{-2}K^{-1}$) (left panel) and absolute vorticity and angular momentum, M (contours) (right panel) as a function radius (horizontal axis, which is linear in radius and runs from 0 to 200 km) and potential temperature (vertical axis), through the center of Hurricane Irma on 6 September 2017, 8 UTC, from a simulation with the non-hydrostatic cloud-resolving limited area prediction model, HARMONIE (KNMI) with a grid size of 3.2 km. Courtesy of Sander Tijm and Jasper de Jong (2020).

PROBLEM 7.1 In how far is the zonal mean zonal wind in balance and what causes departures from balance?

Equation 7.1 has more than one equilibrium solution. In other words, the balanced zonal mean zonal wind, $[u]$, can take on different values for the same meridional gradient of the Montgomery streamfunction. Investigate the relation between the meridional gradient of the Montgomery streamfunction and the zonal mean zonal wind in the Northern Hemisphere, in one month in winter and in one month in summer, using the ERA-Interim re-analysis on isentropic levels. Compare your results to the solution of eq. 7.1. Do this for the following

[8] The inverse of the Rossby ratio, i.e. the ratio, F/N, is sometimes referred to as "**Prandtl's ratio of scales**".

[9] In the core of the mature tropical cyclone, Gloria, values of potential vorticity exceeded 50 PVU (Shapiro, L.J., and J.L. Franklin, 1995: Potential vorticity in hurricane Gloria. **Mon.Wea.Rev., 123**, 1465-1475.

three isentropic surfaces, corresponding to θ=350 K, θ=475 K and θ=600 K. Departures of $[u]$ from the balanced wind are caused by eddy meridional fluxes of potential vorticity substance (**section 1.26**), which give rise to meridional accelerations. Explore the relation between the zonal mean meridional wind, $[v]$, and the zonal mean eddy meridional flux of potential vorticity substance, $[v^*\zeta^*]$. Compare your results to the left panel of **figure 7.19**.

PROBLEM 7.2. **Does the stratosphere affect the circulation near the Earth's surface?** The potential vorticity anomaly at 850 K (approximately 10 hPa) over the Antarctic Continent, which is displayed in the middle panel of **figure 7.12**, has a very large *diameter* of about 4000 km. Will this anomaly have a significant dynamical effect on the wind at the Earth's surface? Why?

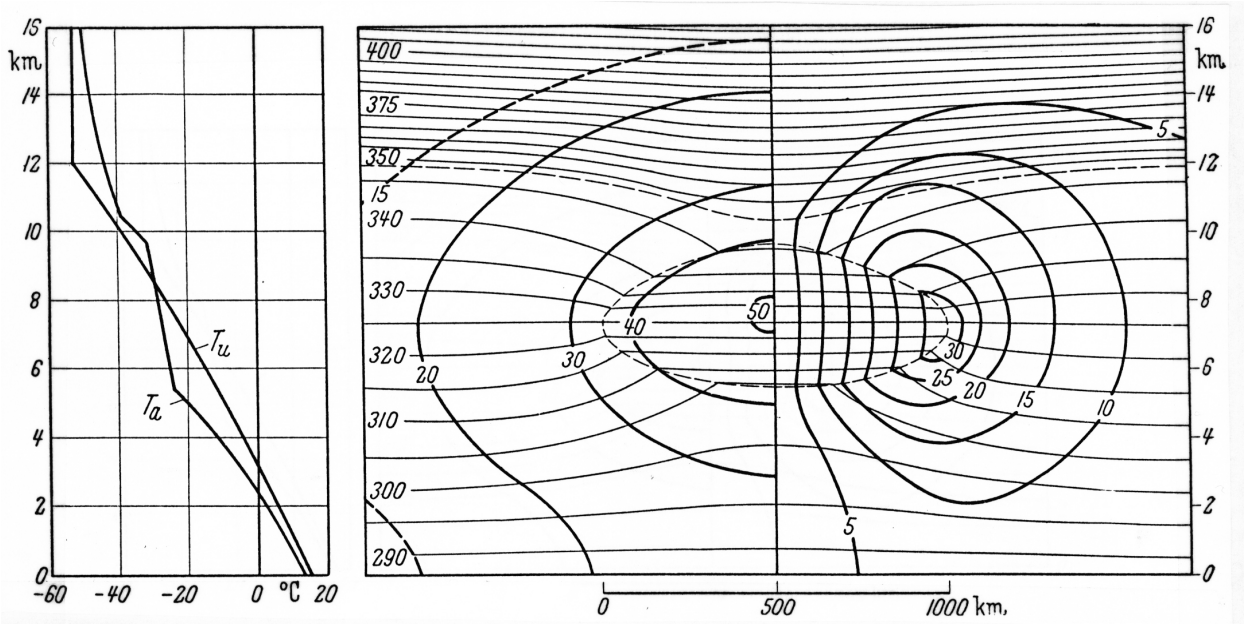

FIGURE 7.14. Model of a cyclone produced by a body of 6 times the normal potential vorticity. Left-hand diagram: temperature distribution on the axis (T_a) and in the undisturbed atmosphere (T_u). Cross-section: thin lines are isentropes labeled in K; heavy lines in the left half indicate the relative depression $(p_u\text{-}p)/p_u$ (per thousand) (p_u is the pressure in the undisturbed atmosphere). Heavy lines on the right are isotachs, labeled in m/s. Figure taken from Eliassen, A. and E. Kleinschmidt, 1957: **Dynamic Meteorology**. In **Encyclopedia of Physics**, vol 48. Edited by S.Flügge and J. Bartels, p1-154.

7.5 Isentropic density distribution in relation to a PV-anomaly

Ernst Kleinschmidt[10] was the first to identify the important relation between potential vorticity and all other variables. His work on this subject was unfortunately largely ignored until more than 10 years after his death in 1970. Kleinschmidt presented a solution of the non-linear potential vorticity inversion equation (7.12) for the case of a cyclone "produced" by a "body of 6 times the normal potential vorticity" (i.e. $Z^+\approx 6$). Kleinschmidt positioned this hypothetical "PV-anomaly" in the upper half of the troposphere. His solution is shown

[10] E. Kleinschmidt, 1950: Über Aufbau und enstehung von Zyklonen, I. **Meteorol.Rundschau, 3**, 1-6. Eliassen, A. and E. Kleinschmidt, 1957: **Dynamic Meteorology**. In **Encyclopedia of Physics**, vol 48. Edited by S.Flügge and J. Bartels, p1-154.

in **figure 7.14**. This figure demonstrates that a positive potential vorticity anomaly is associated with a cyclonic circulation which indeed penetrates vertically and horizontally into the environment of the anomaly, as indicated by the linear analysis in the previous section. The **isentropes are attracted towards the centre of the PV- anomaly**, implying that the static stability is increased within the anomaly and decreased above and below the anomaly. The latter fact can easily be deduced from eq. 7.17b, which, with $Z^+=0$ (i.e. outside the anomaly) becomes

$$\boxed{\zeta^* = \sigma^*}. \qquad (7.31)$$

Therefore, a cyclonic circulation (with $\zeta^+>0$), which is induced remotely by a positive PV-anomaly, leads to a remote *positive* isentropic density anomaly (with $\sigma^+>0$), i.e. a reduction of the static stability above and below the PV-anomaly.

The iterative numerical solution of the PV-inversion equation (7.12) for a given distribution of potential vortcity, Z, consists of two embedded loops. First a solution, $u_1(y,\theta)$, is found iteratively (**Box 7.3**) for a fixed (reference) value of $f_{loc}=f(y)$ and with $\sigma=\sigma_{ref}(y,\theta)$ on the r.h.s. of (7.12). Second, f_{loc}, and σ are corrected, using the first tentative solution $u_1(y,\theta)$, together with the given distribution of Z. With these new values of f_{loc} and σ, however, the first tentative solution $u_1(y,\theta)$, does not obey eq. 7.12. This requires a repetition of the "inner" iteration loop to find a new solution: $u_2(y,\theta)$. The next (second) tentative solution, $u_2(y,\theta)$, deviates less from the real solution than the previous tentative solution. The procedure is repeated until a prescribed convergence criterion is satisfied, i.e. the difference between u_n and u_{n+1} is smaller than a prescribe value at all grid points. The numerical details are given in **Box 7.3**.

When correcting σ (in the "outer" loop), we must require that the mass lying between two isentropic surfaces be the same as in the **horizontally homogeneous reference state**, i.e. as in the horizontally averaged state. On each isentrope we must therefore require that (eq. 7.15):

$$\int \sigma \cos\phi d\phi = \sigma_{ref} \int \cos\phi d\phi \ . \qquad (7.32)$$

Although it is not clear how Kleinschmidt solved the PV-inversion equation[11] he was nevertheless able to draw the following three general conclusions (**figures 7.14** and **7.15**).

1. **Within an isolated air mass with abnormal potential vorticity the static stability as well as the absolute vorticity deviate from the normal in the same sense as the potential vorticity**.

2. In gradient wind equilibrium, an air mass of relatively high potential vorticity establishes a cyclone. **Below this air mass, the isentropic surfaces are raised; above this air mass they are depressed** (**figure 7.15**). Hence the cyclone has a "cold core" below and a "warm core" above the PV-anomaly. If the "producing PV-anomaly" is located just above the earth's surface, as is illustrated in **figure 7.13**, we obtain a cyclone that is warm throughout the atmosphere.

[11] Note that we have not discussed boundary conditions yet. This is the subject of section 7.9.

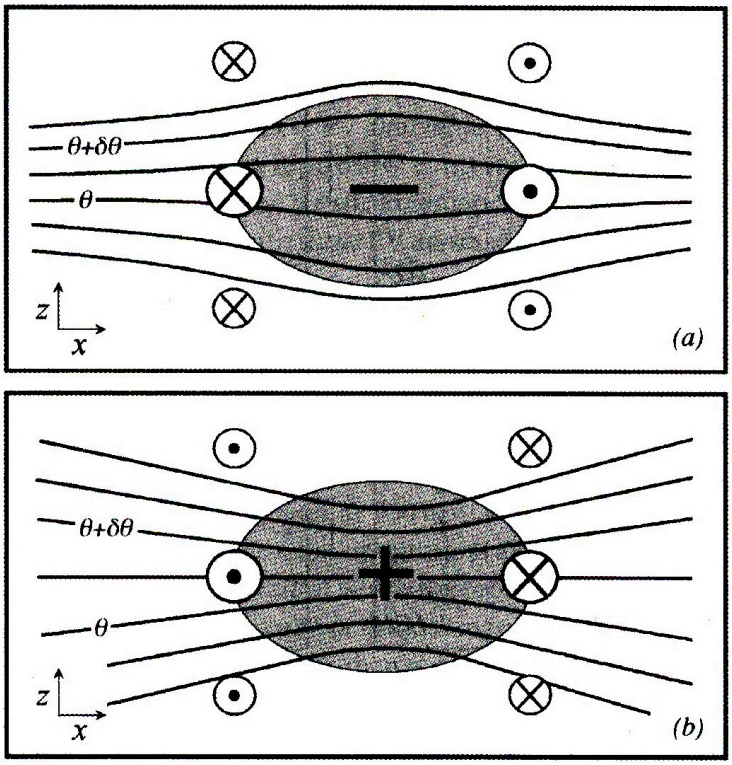

FIGURE 7.15. The isentropes and circulation for idealised negative (a) and positive (b) PV-anomalies. Gray shaded area delineates the PV-anomaly and thin solid lines are isentropes. Wind into the page is indicated by a cross, while wind out of the page is indicated by a dot. Isentropes are repelled by a negative PV-anomaly and attracted by a positive PV-anomaly. Source: Martin, J.E., 2006: **Mid-latitude Atmospheric Dynamics**. John Wiley and Sons. 324 pp. (page 282).

3. An air mass of relatively low potential vorticity gives rise to an anticyclone. The deviations in pressure and temperature have the opposite directional sense to those in cyclones.

The above statements may be reversed. For instance: a balanced cyclone requires a mass of relatively high potential vorticity, or: **a cold air mass only remains cold as long as there are masses of high potential vorticity above it, or masses of reduced potential vorticity below it. When this condition is no longer fulfilled, the air sinks down and loses the character of a cold air mass.**

7.6 PV-inversion: boundary conditions

This section, together with **Box 7.3**, is rather technical and can be skipped if desired. We now return to the problem of finding the zonal average wind velocity from inversion of the zonal average PV-anomaly distribution, using eq. 7.12. The zonal average PV-anomaly distribution is shown in **figure 7.7**.

Equation 7.12 is solved numerically on a domain that runs from the sub-tropics (10° N) to the North Pole, and from an isentrope near the Earth's surface to an isentrope in the upper stratosphere (2250 K). The domain is divided into grid cells with dimensions Δy in the y-direction and $\Delta\theta$ in the θ-direction. A grid point is identified by its index (i, j), where i represents the index in the positive y-direction and j represents the index in the positive θ-

direction. The lower boundary is defined as the lowest computational level that is above the Earth's surface. If we choose the computational levels at regular intervals of $\Delta\theta$=10 K, starting at 240 K, the first level above the Earth's surface at the North Pole in January is 250 K, while the first level above the Earth's surface at 10°N in January is 300 K (**figure 7.16**). For July this difference is much smaller (only 20 K, i.e. 280 K at the North Pole and 300 K at 10°N).

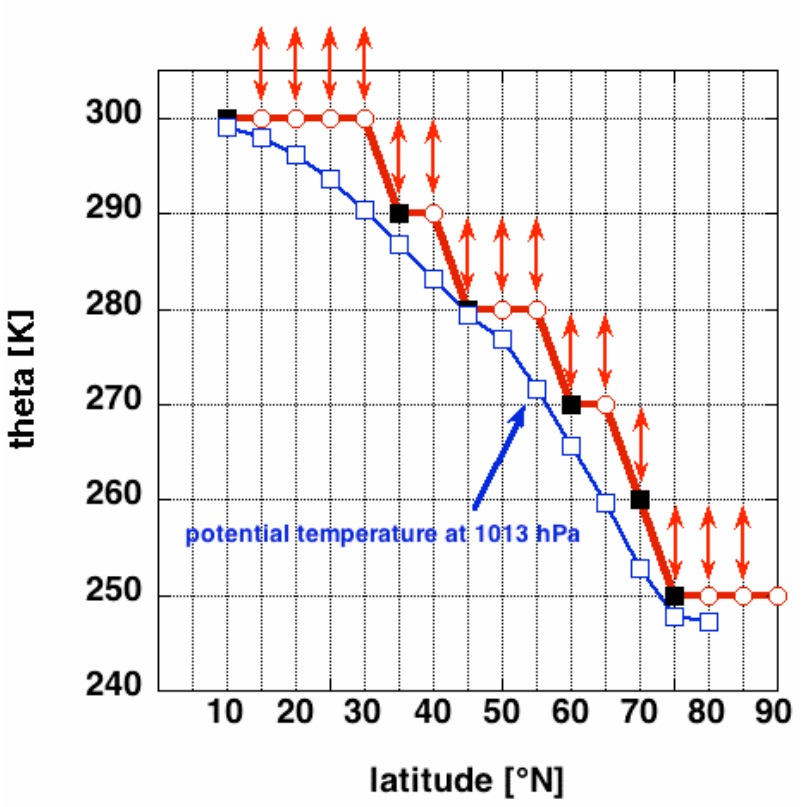

FIGURE 7.16. The approximate position of the Earth's surface (according the CIRA this coincides with p=1013 hPa), relative to the numerical grid in the northern hemisphere in January indicated by the blue line and open squares. The red line indicates the potential temperature of the lowest computational level for January. The black solid squares indicate the grid points that are located at the southern side-boundary of the computational grid. Thermal wind balance is applied to the lowest computational layer (indicated by double arrows) using the CIRA analysis of the isobaric potential temperature gradient (eq. 7.38).

Because isentropes in the "Underworld", below about 300 K, intersect the Earth's surface, the Earth's surface is a "side boundary". In **figure 7.16** the grid points, which are part of this side boundary, are indicated by black squares. Points that represent the lower boundary of the computational grid, but do not represent the side boundary, are indicated by red circles. We employ the circulation theorem to determine $[u]$ at all grid points that are part of the side boundary and do *not* intersect the Earth's surface. At the equatorward boundary the following constraint is imposed. The absolute circulation around this boundary on a specified isentrope is, using Stoke's theorem,

$$C_b = 2\pi a\left(\Omega a\cos\phi_b + [u_b]\right)\cos\phi_b = \iint_A [\sigma][Z]dA, \qquad (7.33)$$

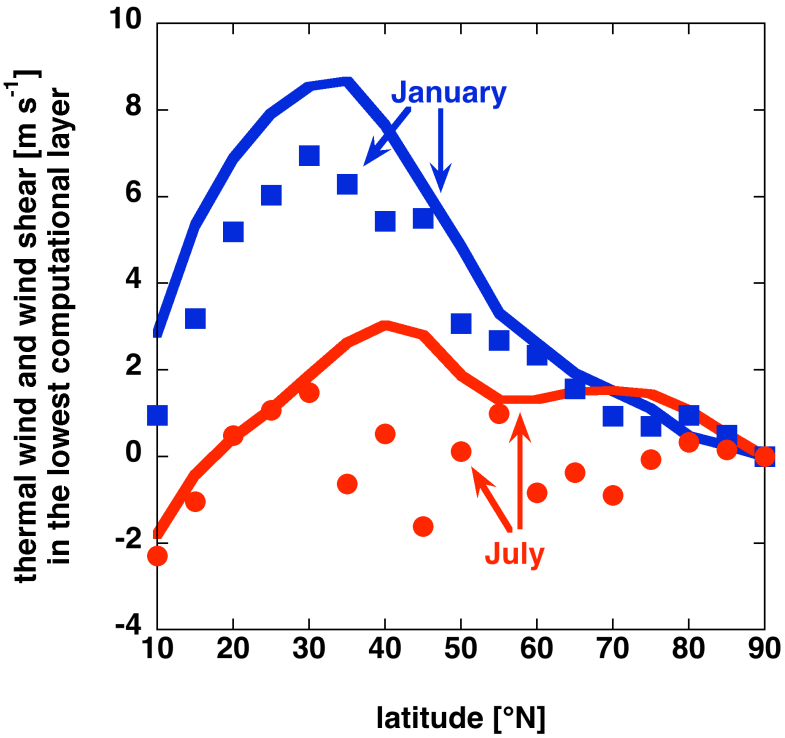

FIGURE 7.17. Thermal wind $\Delta[u]$ in January (blue solid line) and July (red solid line) as a function of latitude in the lowest computational layer (**figure 7.16**), derived from the monthly average zonal average temperature and pressure analysis according to the CIRA, using eq. 7.38 with $f_{loc}=f$. Also shown is the wind shear (m s^{-1}) across the lowest computational layer according to the CIRA (red circles: July; blue squares: January).

where $[u_b]$ is the zonal mean zonal velocity at the boundary and A is the area enclosed by the boundary. If C_b (or $[u_b]$) is given, condition (7.33) imposes restrictions on the possible configurations of $[Z]$. We can also interpret (7.33) the other way around: if we know the distributions of $[\sigma]$ and $[Z]$, we can use (7.33) to determine $[u_b]$ by evaluating

$$[u_b] = -\Omega a\cos\phi + (2\pi a\cos\phi_b)^{-1}\iint_A [\sigma][Z]dA\,. \qquad (7.34)$$

It is customary to identify the lower boundary with the Earth's surface[12], and to use the thermal wind (i.e. the gradient perpendicular to the Earth's surface of $[u]$) as a lower boundary condition, in which case the temperature at the Earth's surface is needed to evaluate the thermal wind at this boundary. Here, however, the lower boundary of the *computational grid* coincides with an isentropic surface (**figure 7.16**). Therefore, we must use the thermal wind equation in θ-coordinates (eq. 7.7). However, at the points where the isentropes intersect the Earth's surface (the black squares in **figure 7.16**), the meridional gradient of the zonal mean Exner function on an isentropic surface (r.h.s. of eq. 7.7) cannot be evaluated numerically, using centered differences (**Box 7.3**). Furthermore, the CIRA-temperature is given on isobaric surfaces. Therefore, we apply a coordinate transformation using the following identities:

[12] Thorpe, A.J., 1985: Diagnosis of balanced vortex structure using potential vorticity. **J.Atmos.Sci.**, **42**, 397-406.

$$d\theta = \left(\frac{\partial\theta}{\partial y}\right)_p dy + \left(\frac{\partial\theta}{\partial p}\right)_y dp \text{ and } dp = \left(\frac{\partial p}{\partial y}\right)_\theta dy + \left(\frac{\partial p}{\partial \theta}\right)_y d\theta \tag{7.35}$$

(assuming that θ is a function of y and p and that p is a function of y and θ). On an isentrope (constant θ) the identities in (7.35) reduce to

$$0 = \left(\frac{\partial\theta}{\partial y}\right)_p dy + \left(\frac{\partial\theta}{\partial p}\right)_y (dp)_\theta = \left(\frac{\partial\theta}{\partial y}\right)_p dy + \left(\frac{\partial\theta}{\partial p}\right)_y \left(\frac{\partial p}{\partial y}\right)_\theta dy = \left(\frac{\partial\theta}{\partial y}\right)_p dy - \frac{1}{g\sigma}\left(\frac{\partial p}{\partial y}\right)_\theta dy$$

so that (*omitting the square brackets*)

$$\left(\frac{\partial p}{\partial y}\right)_\theta = g\sigma\left(\frac{\partial\theta}{\partial y}\right)_p . \tag{7.36}$$

With this and with eq. 6 of **Box 7.1**), we find that

$$\left(\frac{\partial\Pi}{\partial y}\right)_\theta = \frac{c_p\kappa}{p_{ref}}\left(\frac{p}{p_{ref}}\right)^{\kappa-1}\left(\frac{\partial p}{\partial y}\right)_\theta = \frac{g\sigma c_p\kappa}{p_{ref}}\left(\frac{p}{p_{ref}}\right)^{\kappa-1}\left(\frac{\partial\theta}{\partial y}\right)_p . \tag{7.37}$$

Therefore, the numerical (finite difference) approximation of (7.7), applied to the lowest computational layer, indicated by the double arrows in **figure 7.18**, is

$$\Delta[u] = -\Delta\theta\left\langle\frac{1}{f_{loc}}\left(\frac{\partial[\Pi]}{\partial y}\right)_\theta\right\rangle = -\frac{gc_p\kappa\Delta\theta}{(p_{ref})^\kappa}\left\langle\frac{[\sigma]p^{(\kappa-1)}}{f_{loc}}\left(\frac{\partial[\theta]}{\partial y}\right)_p\right\rangle . \tag{7.38}$$

The outer brackets in eq. 7.38 indicate an average over the lowest computational layer above the surface. Except if stated otherwise, it is assumed in (7.38) that $f_{loc} = f$.

Figure 7.17 shows a graph of the thermal wind, $\Delta[u]$, in the lowest layer with "thickness" $\Delta\theta$=10 K, computed form (7.38), using the CIRA-analysis of the potential temperature on the lowest two isobaric surfaces in the CIRA data set (1013 hPa and 788.93 hPa), for January and for July. The strongest January average low-level thermal wind in the lower troposphere is observed in the subtropics at 35°N. In July the maximum thermal wind is shifted somewhat northward. Furthermore, the low level thermal wind is negative in the tropics north of the equator in July, indicating that the equator is cooler near the Earth's surface than the subtropics. The actual vertical wind shear, i.e. the difference in zonal wind speed in the lowest computational layer is also shown. The thermal wind is in general greater than the actual vertical wind shear near the Earth's surface, which is very "noisy" in **figure 7.17**, due to the relatively large steps in θ of the lower boundary (**figure 7.18**).

The lower boundary condition (on $[u]$) is imposed, using (7.38), by specifying $\Delta[u]$ in the lowest layer. The boundary conditions at the North Pole is $[u]$=0. At the upper boundary, at θ=2250 K, $[u]$ is prescribed according to the CIRA.

Box 7.3 PV-inversion: numerical method

Eq. 7.12 is approximated for each grid point [*i*, *j*] (**figure 7.16**) using a **finite difference approximation**. The first term on the left hand side of (7.12) is approximated by (*omitting square brackets*)

$$\frac{\partial^2 u}{\partial y^2} \approx \frac{1}{(\Delta y)^2}\left\{u[i+1,j]+u[i-1,j]-2u[i,j]\right\} \qquad (1)$$

The second term on the left hand side of (7.12) is approximated by

$$-\frac{\partial}{\partial y}\left(\frac{u\tan\phi}{a}\right) = -\frac{\tan\phi}{a}\frac{\partial u}{\partial y} - \frac{u}{a}\sec^2\phi \approx -\frac{\tan\phi[i]}{a}\left\{\frac{u[i+1,j]-u[i-1,j]}{2\Delta y}\right\} - \frac{\sec^2\phi[i]}{a}u[i,j]. \qquad (2)$$

In the third term on the left hand side of (7.12) the second derivative is approximated as follows.

$$\frac{\partial}{\partial\theta}\left(f_{loc}\rho\theta\frac{\partial u}{\partial\theta}\right) \approx \frac{1}{(\Delta\theta)^2}\left\{F^+u_T\left[i,j+\frac{1}{2}\right]-F^-u_T\left[i,j-\frac{1}{2}\right]\right\} \ . \qquad (3)$$

In (3) u_T is the thermal wind within a layer between two isentropic computational levels. For example:

$$u_T[i,j+1/2] = u[i,j+1]-u[i,j]$$

Furthermore,

$$F^- \equiv f_{loc}\left[i,j-\frac{1}{2}\right]\rho\left[i,j-\frac{1}{2}\right]\theta\left[i,j-\frac{1}{2}\right]$$
$$\approx \frac{1}{2}\left\{f_{loc}[i,j]\rho[i,j]\theta[i,j]+f_{loc}[i,j-1]\rho[i,j-1]\theta[i,j-1]\right\}$$

and

$$F^+ \equiv f_{loc}\left[i,j+\frac{1}{2}\right]\rho\left[i,j+\frac{1}{2}\right]\theta\left[i,j+\frac{1}{2}\right]$$
$$\approx \frac{1}{2}\left\{f_{loc}[i,j]\rho[i,j]\theta[i,j]+f_{loc}[i,j+1]\rho[i,j+1]\theta[i,j+1]\right\}$$

so that

$$\frac{\partial}{\partial\theta}\left(f_{loc}\rho\theta\frac{\partial u}{\partial\theta}\right) \approx \frac{1}{(\Delta\theta)^2}\left\{F^+u[i,j+1]+F^-u[i,j-1]-\left(F^++F^-\right)u[i,j]\right\}, \qquad (4)$$

except when *j* corresponds to the level just above the "lower boundary". The thermal wind in the lowest layer is determined by (7.38). Therefore, at the grid points just above the lower boundary we have, instead of (4),

$$\frac{\partial}{\partial\theta}\left(f_{loc}\rho\theta\frac{\partial u}{\partial\theta}\right)\approx\frac{1}{(\Delta\theta)^2}\left\{F^+\left(u[i,j+1]-u[i,j]\right)-F^-\Delta u\right\}. \tag{5}$$

For those interior grid points that are *not* exactly one grid cell above the lower boundary (**figure 7.16**), the left hand side of (7.12) becomes

$$\frac{1}{\Delta y^2}\left\{u[i+1,j]+u[i-1,j]-2u[i,j]\right\}-\frac{\tan\phi[i]}{2a\Delta y}\left\{u[i+1,j]-u[i-1,j]\right\}-\frac{\sec^2\phi[i]}{a^2}u[i,j]$$
$$+\frac{Z[i,j]}{g\Delta\theta^2}\left\{F^+u[i,j+1]+F^-u[i,j-1]-\left(F^++F^-\right)u[i,j]\right\}$$

The right hand side of (7.12) becomes

$$\frac{2\Omega}{a}\cos\phi-\frac{\sigma[i,j]}{2\Delta y}\left(Z[i+1,j]-Z[i-1,j]\right).$$

Numerically approximated, eq. 7.12, applied to all grid points, except those that are located at one grid distance above the lower boundary, becomes

$$u[i,j]+au[i+1,j]+bu[i-1,j]+c\left(F^+u[i,j+1]+F^-u[i,j-1]\right)+d=0\ , \tag{6}$$

where

$$a\equiv\left(\frac{1}{\Delta y^2}-\frac{\tan\phi[i]}{2a\Delta y}\right)e\,, \tag{7}$$
$$b\equiv\left(\frac{1}{\Delta y^2}+\frac{\tan\phi[i]}{2a\Delta y}\right)e\,, \tag{8}$$
$$c\equiv\frac{Z[i,j]}{g\Delta\theta^2}e\,, \tag{9}$$
$$d\equiv\left(-\frac{2\Omega}{a}\cos\phi+\frac{\sigma[i,j]}{2\Delta y}\left\{Z[i+1,j]-Z[i-1,j]\right\}\right)e \tag{10}$$

and

$$e\equiv\left\{-\left(F^++F^-\right)\frac{Z[i,j]}{g\Delta\theta^2}-\frac{2}{\Delta y^2}-\frac{\sec^2\phi}{a^2}\right\}^{-1}.$$

For the grid points that are located at exactly one grid distance above the lower boundary, the numerical approximation of (7.12) is

$$u[i,j] + au[i+1,j] + bu[i-1,j] + cF^{+}u[i,j+1] + d^{*} = 0, \qquad (11)$$

where a, b and c are given respectively, by (7), (8) and (9) with d^{*} now given by

$$d^{*} \equiv \left\{ -\frac{Z[i,j]}{g\Delta\theta^{2}} F^{-}\Delta u - \frac{2\Omega}{a}\cos\phi + \frac{\sigma[i,j]}{2\Delta y}\left\{ Z[i+1,j] - Z[i-1,j] \right\} \right\} e^{*}, \qquad (12)$$

where

$$e^{*} \equiv \left\{ -F^{+}\frac{Z[i,j]}{g\Delta\theta^{2}} - \frac{2}{\Delta y^{2}} - \frac{\sec^{2}\phi}{a^{2}} \right\}^{-1}$$

Eqs. (6) and (11) are solved iteratively, starting with a guess-field, u=0, at all grid points. Evaluating the left hand side of (6) or (11) will produce a residual, ΔR, which should be equal to zero at all points. Obviously, this is not the case with the first guess, except when d or d^{*} (i.e. at least one of the "forcing-terms") is equal to zero.

Comparison of the forcing terms, d and d^{*}, respectively in (10) and (12), suggests that a negative thermal wind, Δu, adjacent to the Earth's surface (i.e. a warm anomaly at the pole) has the same dynamical effect as a positive isentropic gradient of the potential vorticity in the atmosphere (for example, a positive PV-anomaly over the North Pole). The thermal wind adjacent to the Earth's surface is in general positive (**figure 7.17**). Therefore, the **temperature gradient at lower boundary will induce an anticyclonic circulation around the North Pole**, which opposes the cyclonic circulation that is induced by the positive PV-anomalies in the atmosphere. In other words, the circulation induced by the boundary temperature anomaly partly compensates the circulation induced by the interior PV-anomaly (see sections 7.7 and 7.8 for cautionary notes on this interpretation).

By making a new guess, such that

$$u_{new}[i,j] = u_{old}[i,j] - \Delta R\ , \qquad (13)$$

the new residual is reduced to zero at grid point [i, j]. The same procedure is then followed at the neighbouring grid point. This will, however, perturb the solution of the preceding grid point. Therefore, the entire grid needs to be scanned many times. Provided the equation is of the elliptic type, the residuals become smaller at each successive scan of the entire grid. The iteration procedure is stopped when the absolute value of the residual at all grid points is smaller than some prefixed value, after which we compute the associated isentropic density anomaly with (7.17a). Next, a horizontally uniform correction is applied to σ so that the total mass, lying between two isentropic surfaces, is the same as the total mass lying between these two isentropic surfaces in the horizontally homogeneous reference state, i.e.

$$\int \sigma \cos\phi d\phi = \sigma_{ref} \int \cos\phi d\phi \qquad (14)$$

on each isentropic computational level.

The new distribution σ perturbs eq. (7.62), requiring a new guess for u. The program consists of two embedded iteration loops: the inner loop is concerned with finding u for fixed σ, while the outer loop is concerned with correcting σ for the value of u that is

obtained from the inner loop, imposing the condition of mass conservation. Convergence criteria on both u and σ must be set. This method is called "**successive relaxation**", because the new guess of u is used immediately to evaluate the residual at the neighboring grid point. In the mathematical literature this method is known as "**Gauss-Seidel iteration**". A slightly more sophisticated version of this method is known as "**successive over-relaxation**" (SOR). In this method the residual in (13) is multiplied by a factor that is slightly greater than 1. Usually convergence is faster for SOR. However, in the case at hand, SOR does not converge as monotonically as is the case with "ordinary" successive relaxation.

7.7 Attribution of jets to PV-anomalies by piecewise PV-inversion

This section discusses the solution of the PV-inversion eq. 7.12 for the zonal mean PV-distribution of both January and July (**figure 7.7**) for the northern hemisphere. The solution for January is shown in **figure 7.18** (left panel). For comparison, the analysed zonal wind (according to the CIRA) is shown in the right panel of **figure 7.18**. Both the subtropical jet at about 30°N and 350 K and the stratospheric polar night jet, at about 65°N and above 450 K, appear in the inverted wind field with about the right magnitude. The greatest differences between the analysed wind field and the inverted wind field (left panel of **figure 7.19**) are found at mid-latitudes in the layer between the two major PV-anomalies (between 350 and 450 K) as well as near the earth's surface. Turbulent eddies in the boundary layer and mixing of PV by planetary waves in the mid-latitude higher troposphere and lower stratosphere, presumably, induce relatively large deviations from thermal wind balance in these regions of the atmosphere, thereby explaining these differences.

The subtropical jet and the polar night stratospheric jet can be attributed to particular features of the PV-field by **piecewise PV-inversion**. The technique of piecewise PV-inversion is, however, not useful if we cannot superpose the wind fields of the piecewise inverted PV-anomalies and retrieve the original wind field. Because of the non-linearity of the PV-inversion eq. (7.12), it is the question whether this "**superposition-principle**" is valid.

As a test of the validity and applicability of the technique of piecewise PV-inversion, the PV-anomaly field is split into two portions: the first portion consists of all PV-anomalies below θ=480 K, *together with* the lower boundary temperature anomaly (a boundary temperature anomaly is sometimes also refered as a potential vorticity anomaly), while the second portion consists of the stratospheric PV-anomaly above θ=480 K, including the upper boundary condition on the zonal mean zonal wind. The question why the Ex-UTLS PV-anomaly is inverted together with the lower boundary temperature anomaly is explained later.

The PV-inversion equation is solved for both anomaly fields separately. After adding the two inverted wind fields we should retrieve the wind field obtained from inversion of the full PV-field, shown in the left panel of **figure 7.18**. The right panel of **figure 7.19** shows that this is nearly so. We can thus **attribute particular features of the wind field in the winter hemisphere to features of the PV-anomaly field**.

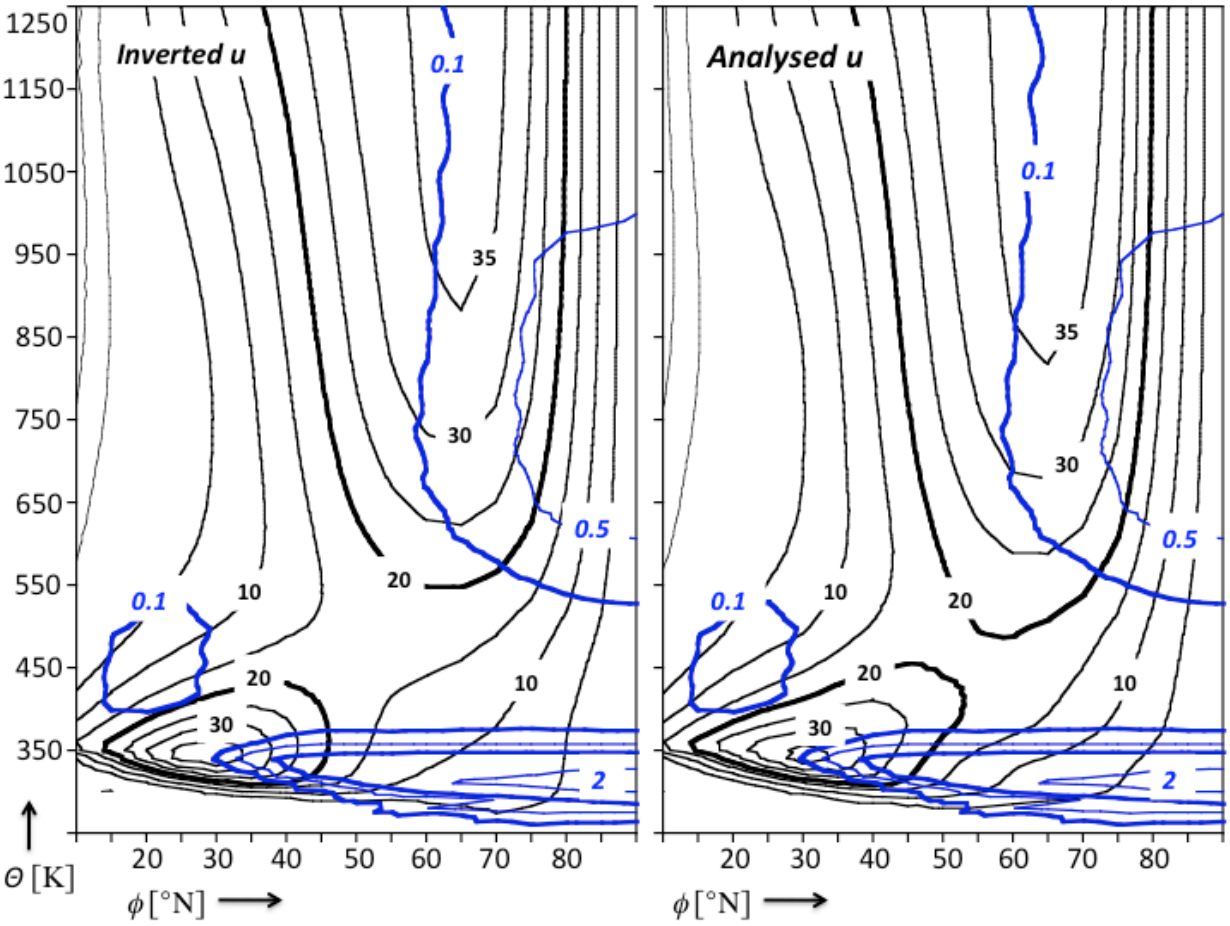

FIGURE 7.18. The zonal average, monthly average zonal wind velocity as a function of potential temperature and latitude (black contours, labeled in m s^{-1}) in January, derived from PV-inversion (left panel) and according to the CIRA (right panel). The normalised PV-anomalies that "induce" this wind field are shown in blue (only positive values are contoured). Labels are given in non-dimensional units. The isopleths corresponding to 0.1 and 1 non-dimensional unit are drawn thick; the isopleths corresponding to 0.5, 2 and 3 non-dimensional units are drawn thin. For more details of the structure of these anomalies, see **figure 7.7**.

The wind field, which is induced by both the Ex-UTLS PV-anomaly *and* the lower boundary temperature anomaly, is shown in the left panel of **figure 7.20**. The strength of the subtropical jet is explained almost fully by the presence of the Ex-UTLS PV-anomaly *and* the lower boundary temperature anomaly. In other words, the upper stratospheric PV anomaly (above θ=480 K) has very little effect on the zonal mean subtropical jet.

In contrast to this, the Ex-UTLS PV-anomaly does have a significant effect on the strength of the stratospheric jet below 1250 K. If we remove both the PV-anomalies below θ=480 K (i.e. the Ex-UTLS PV anomaly) *and* the surface temperature anomaly (i.e. we put $\Delta[u]$=0 in eq. 7.38) and solve the PV-inversion equation with the PV-anomalies above θ=480 K retained, we get the result that is shown in the right panel of **figure 7.20**.

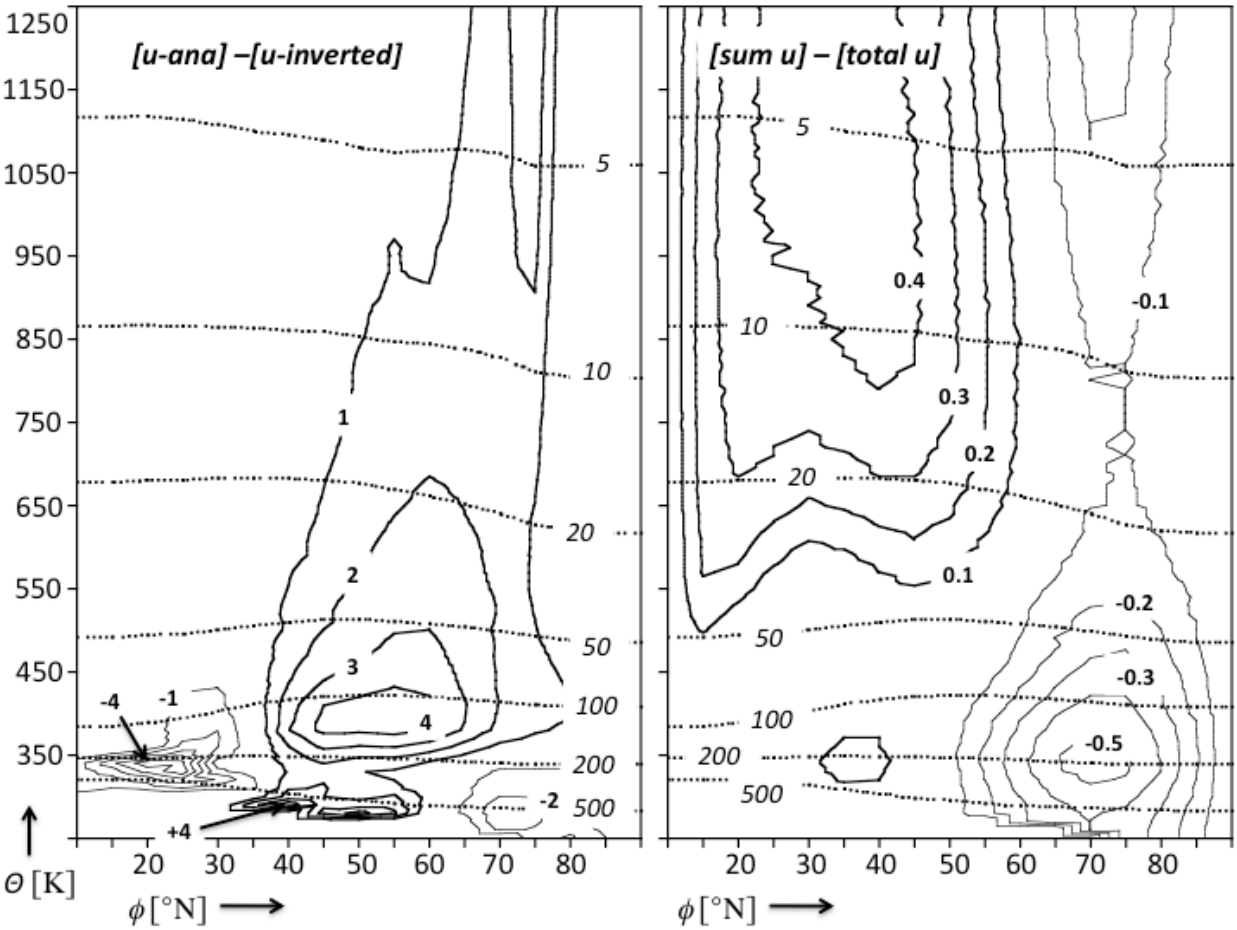

FIGURE 7.19. Left panel: difference between analysed zonal mean zonal wind and inverted zonal mean zonal wind for January (labeled in units of m s^{-1}). Note that the ***analysed*** eastward zonal wind speed exceeds the ***balanced*** zonal wind speed by several m/s in the middle latitudes, while the opposite the case over the Pole and close to the subtropical jet stream. Right panel: difference between the sum of two piecewise inverted wind fields, shown in **figure 7.20**, and the wind field obtained from inversion of the total PV-field, shown in the left panel of **figure 7.18**. Labels are in units of m s^{-1}. The inverted pressure field is also shown (dotted lines labeled in units of hPa).

Apparently, the presence and the general features of the polar night stratospheric jet are explained by the PV-anomaly above θ=480 K, but not its full strength. As stated before, and illustrated in the right panel of **figure 7.19**, the sum of the two wind fields, which is shown in **figure 7.20**, is nearly identical to the wind field resulting from inversion of all anomalies, shown in left panel of **figure 7.18**.

Figure 7.21 (left panel) shows the wind field induced by the PV-anomaly distribution of July over the northern hemisphere. The analysed wind (according to the CIRA) is shown on the right in the same figure. Again, the agreement between analysed and inverted zonal wind speeds is very good. But, can we still attribute the subtropical jet in July only to the Ex-UTLS PV anomaly together with the lower boundary temperature anomaly? The following section addresses this question.

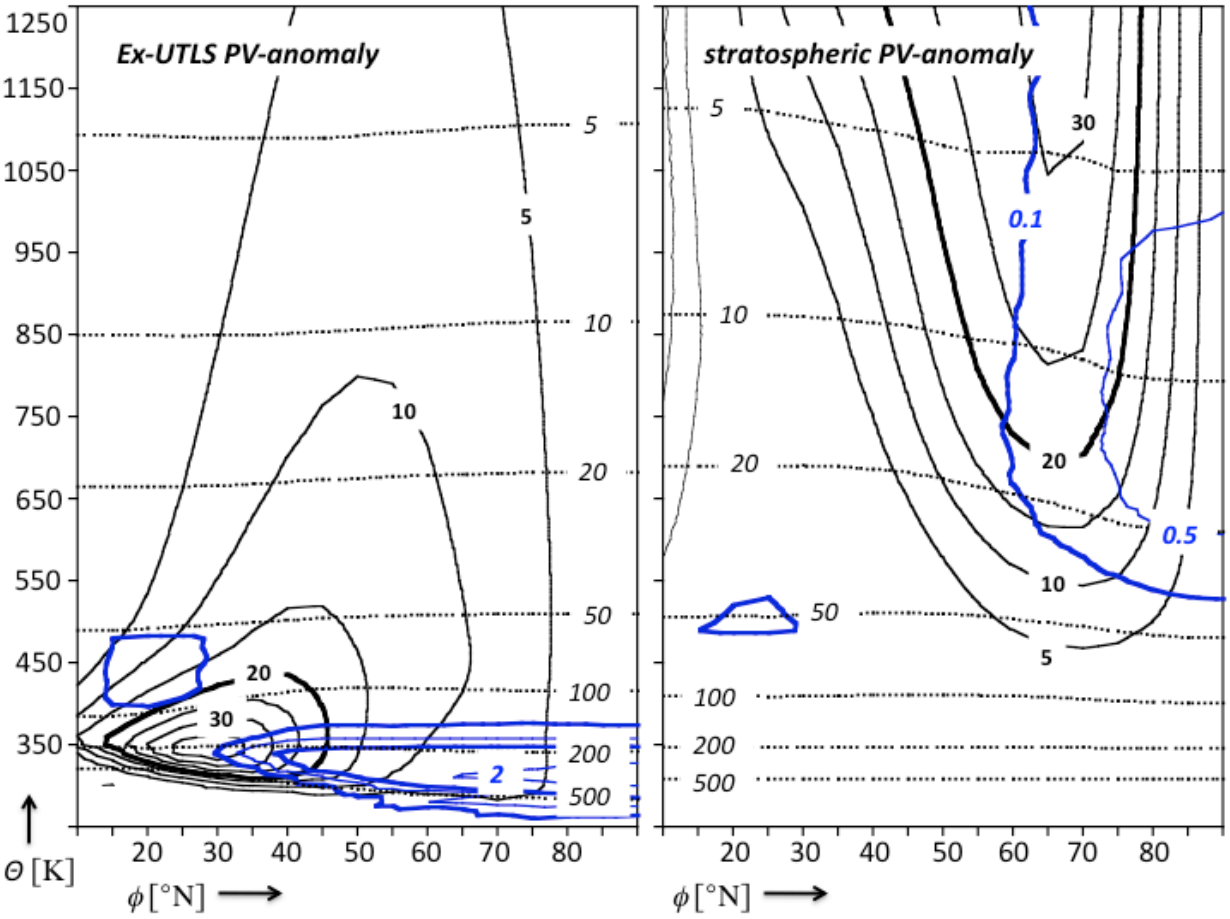

FIGURE 7.20. The zonal average, January average zonal wind velocity (black contours labeled in m s^{-1}) and pressure (dotted lines, labeled in hPa) as a function of potential temperature and latitude, derived from piecewise PV-inversion. The left panel shows the result when the Ex-UTLS PV-anomaly and the surface temperature anomaly are retained (i.e Z^{+}=0 for θ>480 K). The right panel shows the result when only the polar cap upper stratospheric PV-anomaly is retained (i.e Z^{+}=0 for $\theta \leq 480$ K and Δu=0) and the zonal wind according to the CIRA is imposed at the top boundary at 2250 K. The PV-anomalies that are retained in the inversion are shown in blue and labeled in non-dimensional units as in **figure 7.18** (only positive values are contoured).

7.8 Piecewise PV-inversion and the lower boundary condition

Because of the relative proximity of the negative stratospheric PV-anomaly to the Ex-UTLS PV anomaly in July, the answer to the question posed at the end of the previous section is: "*probably not*". But there is a complication here. The removal of a PV-anomaly, in particular a PV-anomaly that is associated with a large isentropic density anomaly, implies an isentropic redistribution of mass, which leads to a change of pressure at the lower boundary. Since the lower boundary is defined at a specific isentropic level, a change of the pressure distribution at the lower boundary implies a different thermal wind at this boundary (eq. 7.7). In other words, it is **physically inconsistent to invert particular portions of the PV-field with a lower boundary condition that is only appropriate for the inversion of the total PV-field**. This section investigates the effect on the lower boundary thermal wind of the removal of PV-anomalies that are associated with large isentropic density anomalies.

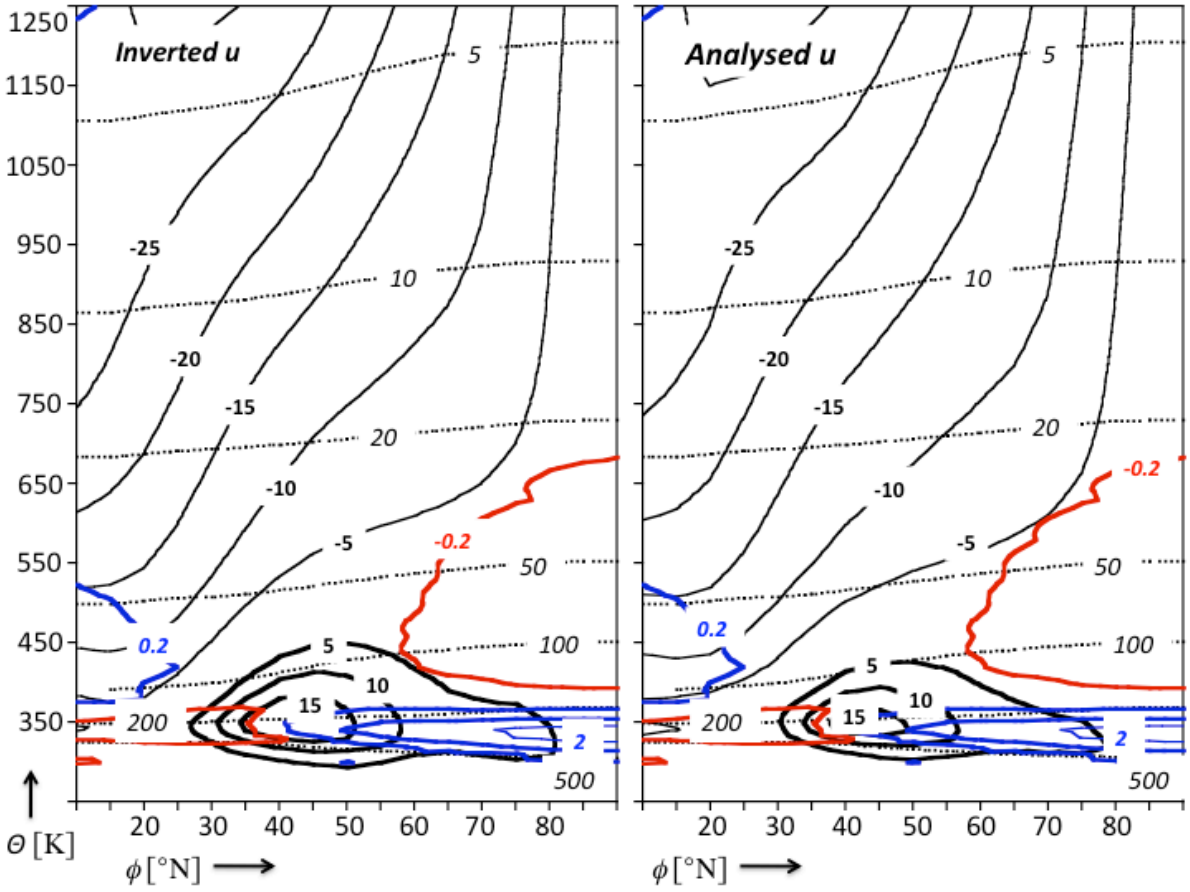

FIGURE 7.21. The zonal average, monthly average zonal wind velocity as a function of potential temperature and latitude (black contours, labeled in m s^{-1}) in July derived from PV-inversion (left panel) and according to the CIRA (right panel). The normalized PV-anomalies that "induce" this wind field are shown in colours (negative values in red; positive values in blue; labeled in non-dimensional units as in **figure 7.18**). Also shown is pressure (dashed lines, labeled in hPa).

The northern hemisphere polar cap stratospheric PV-anomaly in January is associated with $\sigma^{+}\approx$-0.2 between 20 hPa and 5 hPa, pole-ward of about 70° latitude (**figure 7.9**, upper panel), implying a mass-anomaly which represents only about 0.3 % of the hydrostatic pressure at the Earth's surface. Therefore, removal of this PV-anomaly has a negligible effect on the surface pressure and, therefore, also a negligible effect on the thermal wind at the lower boundary. The Ex-UTLS PV-anomaly, however, is associated with $\sigma^{+}\approx$-0.5 between 500 hPa and 200 hPa in the extra-tropics, poleward of about 35° latitude (**figure 7.9**, upper panel), implying a negative mass anomaly which represents about 15% of the hydrostatic pressure at the Earth's surface. So, by removing the Ex-UTLS PV-anomaly we are effectively moving a significant portion of the mass of the atmosphere from the tropics to the extra-tropics. Hence, in this case (January in the northern hemisphere) the inhomogeneous lower boundary condition, i.e. the temperature anomaly at the Earth's surface, should be "attributed" partly to the Ex-UTLS PV-anomaly. This is the reason for not inverting the Ex-UTLS PV anomaly by itself but only together with the lower boundary temperature anomaly. In fact, inversion of the positive Ex-UTLS PV-anomaly by itself results in absurdly high balanced cyclonic wind speeds! If only the boundary temperature anomaly is inverted (with no PV-anomalies in the atmosphere), an anticyclonic balanced

wind field with speeds approaching 100 m s^{-1} at the Earth's surface in middle latitudes is obtained [13].

The mass-anomaly, which is associated with the northern hemisphere stratospheric PV-anomalies **above 370 K in July**, is equivalent to a positive hydrostatic pressure-anomaly below 370 K of about 25 hPa over the pole and a negative hydrostatic pressure-anomaly below 370 K of about 8 hPa over the subtropics. Therefore, removal of the stratospheric PV-anomaly must lead to a redistribution of mass with a pressure decrease in the extratropics and a pressure increase in the subtropics, as is shown in **figure 7.22**. On an isentropic surface near to the Earth's surface this appears as a cold anomaly over the pole, which induces an anticyclonic circulation in the troposphere. The importance of this effect is difficult to assess exactly. Yet, a good impression of the amplitude of this effect is obtained by multiplying the surface thermal wind, Δu, in eq. 12 of **Box 7.3** by the ratio of the thermal wind at 300 K (the lowest computational isentropic level that does not intersect the earth's surface) after and before the removal of the stratospheric negative PV-anomaly, and repeating the PV-inversion with the stratospheric negative PV-anomaly removed, with the corrected value of Δu as a boundary condition.

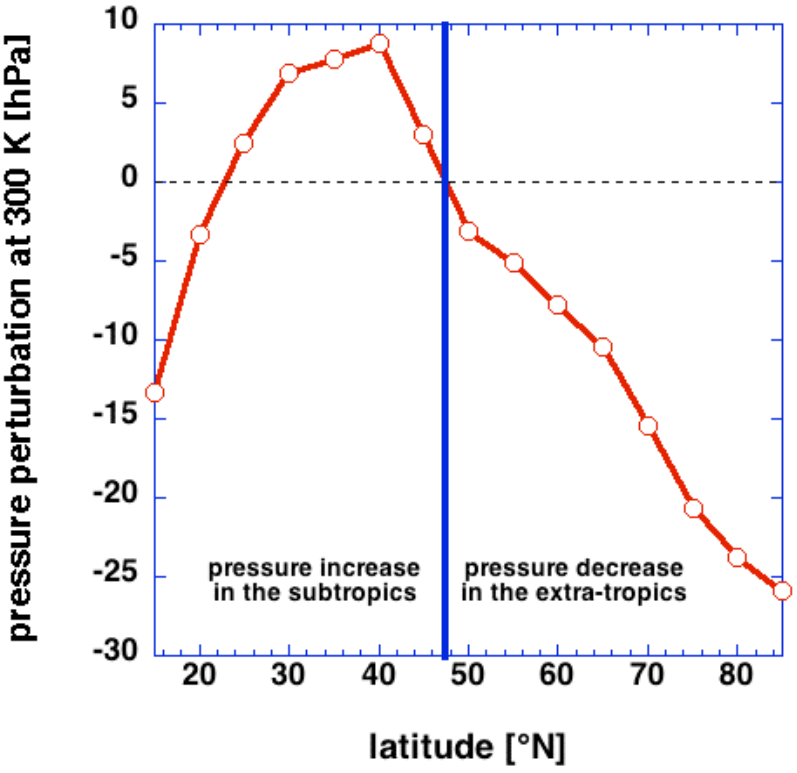

FIGURE 7.22. The zonal average pressure anomaly at 300 K in July in the northern hemisphere, that results after removing the PV-anomaly above 370 K and redistributing the associated mass anomaly, i.e. effectively transferring mass from the extra-tropics to the subtropics. The boundary condition must be corrected for this effect.

[13] These high values are also found by e.g. Holopainen and Kaurola (1991) (their figure 4b) (Holopainen, E. and Kaurola, J., 1991: Decomposing the atmospheric flow using potential vorticity framework. **J.Atmos.Sci**., **48**, 2614-2625.

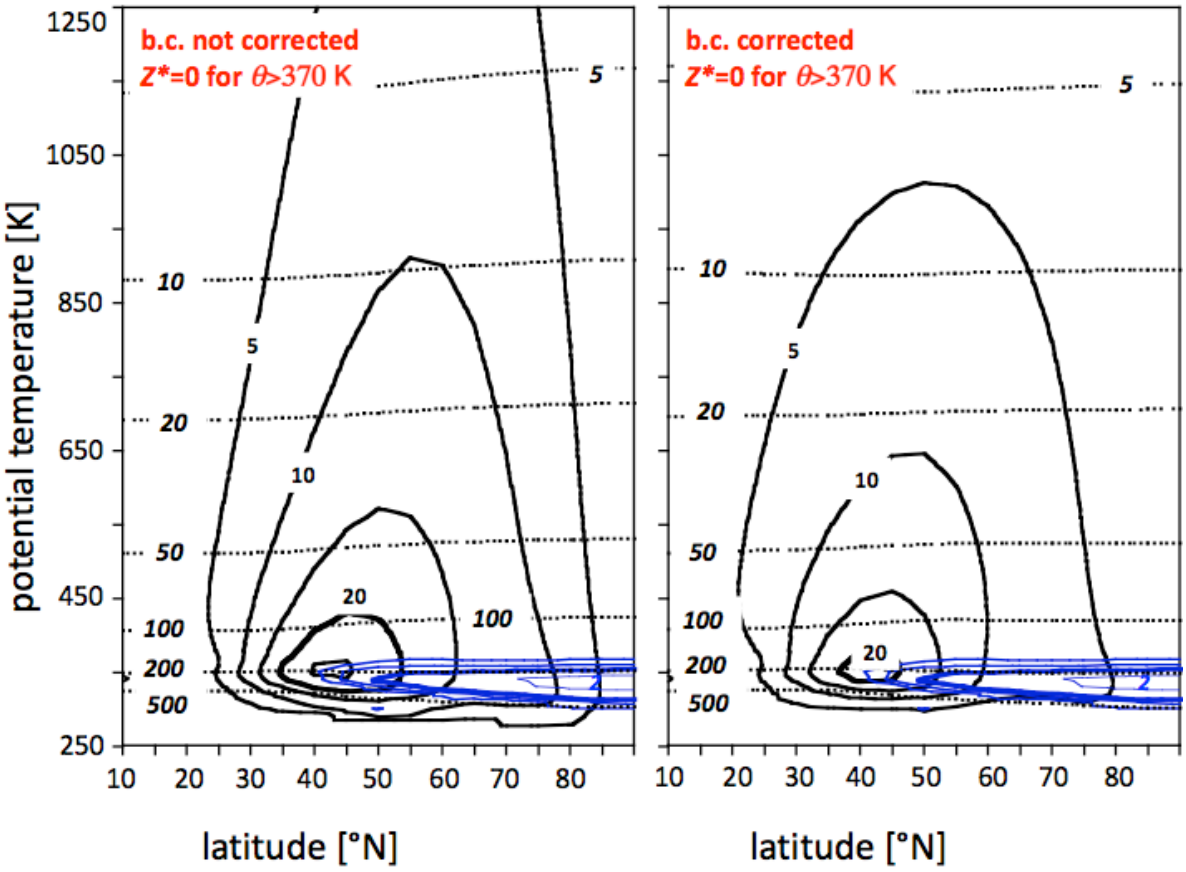

FIGURE 7.23. The zonal average, July average zonal wind velocity as a function of potential temperature and latitude (black contours, labeled in m s^{-1}) according to the solution of the PV-inversion when Z^{+}=0 for θ>370 K (only positive values of Z^{+}, labeled in non-dimensional units as in **figure 7.18**, are shown in blue). Left panel: case where the thermal wind at the lower boundary is not corrected; Right panel: case where the thermal wind at the lower boundary is corrected for the redistribution of mass.

The results of the piecewise PV-inversion for July are shown in **figure 7.23**. The left panel shows the result of the uncorrected inversion, while the right panel shows the result of the corrected inversion. Clearly, the net effect of removing the stratospheric negative PV-anomaly is to intensify the westerlies in the troposphere and lower stratosphere.

The effect of the redistribution of mass, due to the removal of the negative stratospheric PV-anomaly, on the lower boundary condition cannot be neglected in this case, as opposed to the winter (January) case. We may conclude that the negative stratospheric PV-anomaly above 370 K is at least partly responsible for the relatively weak summer westerlies in the troposphere and lower stratosphere.

7.9 "PV-theta viewpoint" of the zonal mean state

This chapter investigates the "PV-θ viewpoint" of the zonal mean state of the atmosphere. PV-anomalies are defined with respect to a reference state that is at rest with respect to the rotating earth. A diagnosis is presented of the zonal mean potential vorticity anomalies in January and July, derived from the COSPAR International Reference Atmosphere (CIRA),

focussing on interesting PV-features, in particular in the upper troposphere and the lower stratosphere.

Two positive PV-anomalies catch the eye in this analysis. One of these PV-anomalies, which is referred to as the "Ex-UTLS PV-anomaly", is located between the pole and 30° to 40° latitude at levels between 310 and 360 K. The Ex-UTLS PV-anomaly is positive throughout the whole year and it exhibits a very weak seasonal cycle. Piecewise PV-inversion demonstrates that the balanced dynamical "response" to this positive PV-anomaly consists of a subtropical eastward jet. The second PV-anomaly, i.e. the stratospheric PV-anomaly, exhibits a strong seasonal cycle. In summer the the stratospheric PV-anomaly is negative and is located just above the Ex-UTLS PV-anomaly. In winter the stratospheric PV-anomaly is positive and, in the northern hemisphere, it is located above 500 K (20 km above sea level) and poleward of 50°-latitude. Piecewise PV-inversion reveals that this stratospheric PV anomaly induces the stratospheric polar vortex. Part of the wind field in the polar winter stratospheric vortex, however, is induced by the Ex-UTLS PV-anomaly.

In the northern hemisphere winter the layer between 360 K and 500 K is characterised by a positive PV-anomaly at low latitudes together with negative PV anomaly at mid-latitudes, indicating that meridional PV-mixing by breaking planetary waves, which is characteristic for the "surf-zone" in the stratosphere, is very important in this layer.

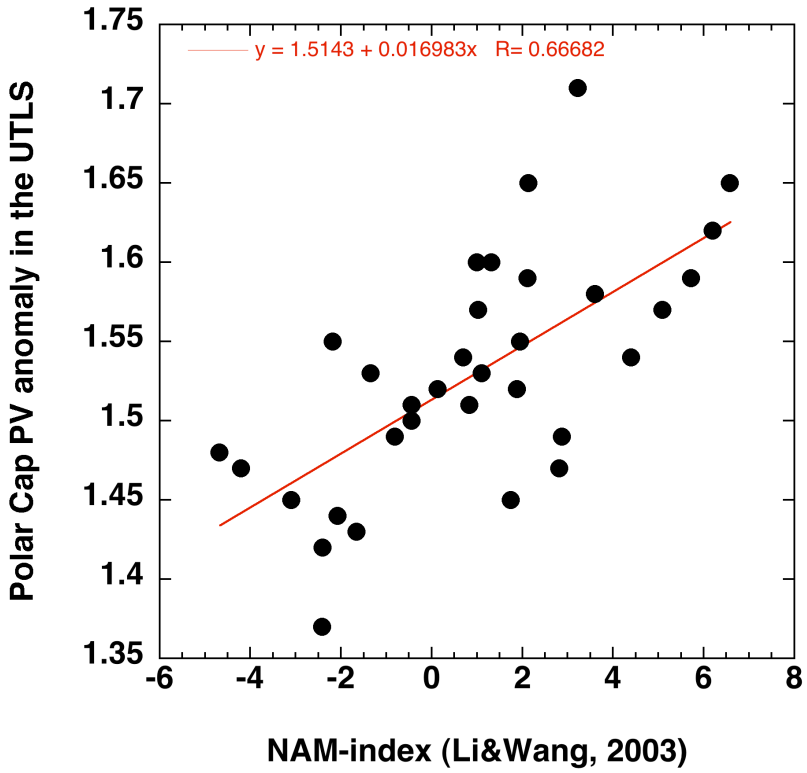

FIGURE 7.24. Scatter plot of the monthly mean (January of the years 1979 to 2011) polar cap normalized potential vorticity anomaly, Z^+, averaged over the layer between 300 K and 370 K, north of 65°N, and the monthly mean Northern Annular Mode (NAM) Index, which is defined as the difference in the normalized monthly zonal-mean sea level pressure between 35°N and 65°N. The red line represents the best linear fit to the 33 points with a correlation coefficient of 0.67. The monthly mean potential vorticity is derived from the ERA-Interim reanalysis (http://data-portal.ecmwf.int/data/d/interim_full_moda/levtype=pt/).

A complication remains when applying *piecewise* PV-inversion to large-scale PV-anomalies that are manifest strongly as mass-anomalies. This complication is related to the interpretation of the lower boundary condition. The surface hydrostatic pressure gradient is determined by mass-anomalies in association with the PV-anomalies. Removing a PV-anomaly under the condition of mass conservation (i.e. redistributing its mass anomaly) implies a change of hydrostatic surface pressure and, therefore, also a change of the thermal wind at the surface. Therefore, if a PV-anomaly, which is associated strongly with a mass-anomaly, such as the Ex-UTLS PV-anomaly, is removed artificially, the surface thermal wind must be adjusted accordingly. In the northern hemisphere winter (e.g. in January), the only significant isentropic zonal mean mass anomaly is that which is associated with the Ex-UTLS PV-anomaly. This implies that the Ex-UTLS PV-anomaly is inextricably connected to the lower boundary temperature/pressure anomaly distribution. This connection can clearly be seen in **figure 7.24**, which demonstrates that the surface NAM-index in January (**section 1.27**) is positively correlated with the average normalised polar cap potential vorticity anomaly in the UTLS. An analysis of the mass- and PV-budget of the layer between 300 K and 380 K and processes that determine this mass- and PV-budget, will probably provide clues to the answer to the question which processes lead to annular mode variability. This variability is very likely determined by meridional mixing of potential vorticity in the ex-UTLS and in the lower stratospheric surf zone. This mixing is due to vertical propagation of planetary Rossby waves, a topic which will be treated in **chapter 11**.

The ex-UTLS, between θ=310 K and θ=370 K, stands in "adiabatic contact" with the tropical troposphere and the upper outflow branch of the Hadley circulation, which is driven by release of latent heat in the ITCZ. Therefore, the tropics may also play a large role in determining the PV-distribution in the layer between θ=310 K and θ=370 K, which is referred to as the "Middleworld". Chapter 12 aims to identify more precisely how processes, such as radiative transfer, latent heat release in the tropical Hadley circulation and "planetary wave drag" act together to maintain the observed PV-distribution.

Hopefully this chapter has provided a feel for the character of the relation between the potential vorticity field and the temperature- and wind-field.

PROBLEM 7.3. **The surf zone: zonal mean zonal wind and mass distributions that result from meridional mixing of potential vorticity**

The PV-dstribution in the layer between θ=370 K and θ=550 is characterised by a reversed isentropic gradient of Z^+ (**figure 7.7**). This is the consequence of meridional "mixing" of potential vorticity by eddies under the constraint of material conservation of potential vorticity. Potential vorticity mixing, which occurs in a retricted band of latitudes, called "the surf zone", makes the zonal mean potential vorticity uniform within this surf zone and creates merional PV-gradients at the edge of the surf zone, as is indicated schematically in **figure 7.25** (Dritschell and McIntyre (2008); see also Hoskins and James (2014), chapter 18). It is interesting to note that the reference potential vorticity, Z_{ref} (**section 7.3**), depends on latitude. According to the solution of the PV-inversion equation (7.12), assuming homogeneous upper and lower boundary conditions, Z_{ref} is associated with a zonal mean zonal wind, $[u]$=0. Mixing of Z_{ref} in a range of latitudes between the latitudes, ϕ=ϕ_S and ϕ=ϕ_N, will create PV-steps at these latitudes. The isentropic tropopause at =350 K, for instance, is an approximate PV-step, which is established *partly* by inhomogeneous lateral PV-mixing. If the atmosphere adjusts to balance, this will lead to eastward zonal winds at and in the vicinity of the latitudes of the PV-steps.

Perform a detailed investigation of the influence of eddy PV-mixing on the zonal mean

state of the atmosphere. In which way will the zonal wind change when Z_{ref} is mixed, and how will this affect the pressure distribution in isentropic coordinates? For this problem you will need to use the PV-inversion Python-code.

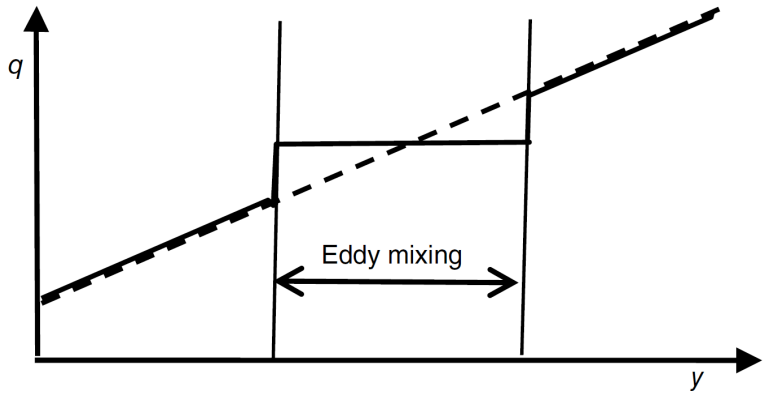

FIGURE 7.25. Schematic illustration of the effect of eddy mixing on the distribution of potential vorticity. The initial monotonically increasing distribution is shown by the dashed line, and the step-like distribution after eddy-mixing by the solid line (Hoskins and James, 2014, figure 18.6).

ABSTRACT OF CHAPTER 7

Chapter 7 is concerned with the **relation between the wind and the distribution of potential vorticity in an atmosphere which is in thermal wind balance**.

It is shown that **thermal wind balance implies that all dynamical fields such as wind and pressure are determined by the distribution of potential vorticity**. This is called the "**Invertibility Principle**" (also introduced in a physically simplified model in chapter 5). According to the solution of the elliptic equation associated with this principle (the **"PV-inversion equation"**), a potential vorticity anomaly is a centre of forcing which induces a **remote wind-response in the atmosphere**. The aspect ratio (horizontal scale divided by the vertical scale) of this wind-response is proportional to the Brunt Väisälä frequency divided by the inertial frequency, which is usually in the order of 100.

Piecewise PV-inversion is introduced as a technique to attribute particular features of the wind field, such as the jets, to particular features of the PV-distribution, such as PV-anomalies.

At first sight the idea of (piecewise) PV-inversion seems conceptually relatively simple. But, unfortunately, the task of finding and applying boundary conditions for the solution of the PV-inversion equation represents a significant complication, with some possible pitfalls, related to the fact that a PV-anomaly is manifest partly as a mass-anomaly.

These ideas are worked out explicitly here for the zonally symmetric state of the atmosphere. The **reference state** PV-distribution is associated with the state of rest. **Two dominant potential vorticity anomalies,** which determine the structure and intensity of the zonally symmetric circumpolar flow, are identified. The potential vorticity anomaly, which induces the eastward winds in the troposphere, including the **subtropical jet**, is the so-called **ex-UTLS PV-anomaly**. This PV-anomaly, which is centred at 330 K (250 hPa), is broad (extending from the pole to the about 30° latitude) and shallow. It can be identified with the extra-tropical tropopause. The **polar winter stratospheric jet** is induced by the **polar cap**

stratospheric potential vorticity anomaly, which is located above 500 K (20 km above sea level) and poleward of 60°-latitude. The positive Ex-UTLS PV-anomaly and the polar night stratospheric positive PV-anomaly can be viewed as the principal **building blocks** of the zonal average atmospheric circulation in winter.

The influence of meridional PV-mixing due to breaking planetary on the zonal average PV-distribution is evident between 400 K and 550 K in the northern hemisphere winter. In summer the dynamical state of the stratosphere is determined by the ex-UTLS PV-anomaly and by a negative PV-anomaly above 400 K.

Further reading

Books

Hoskins, B.J., and I.N.James, 2014: **Fluid Dynamics of the MidLatitude Atmosphere**. John Wiley & Sons, 408 pp. (see chapter 10 for an explanation of potential vorticity (inversion) and chapter 18 for an explanation of the consequences of PV-mixing).

Lackmann, G., 2011: **Midlatitude Synoptic Meteorology**. American Meteorological Society. 345 pp. (see chapters 3 and 4).

Articles

Delden, A.J. van, and Y.B.L. Hinssen, 2012: PV-θ view of the zonal mean state of the atmosphere. **Tellus A** 2012, 64, 18710, http://dx.doi.org/10.3402/tellusa.v64i0.18710. (The material in sections 7.6-7.11 is largely based on this paper)

Fleming, E. L., Chandra, S., Barnett, J. J. and Corney, M. 1990. Zonal Mean Temperature, Pressure, Zonal Wind, and Geopotential Height as Functions of Latitude. **Advances in Space Research 10**, No. 12, 11-59.

Hoskins, B.J., M.E. McIntyre and A.W. Robertson, 1985: On the use and significance of isentropic potential vorticity maps. **Quart.J.R.Met.Soc., 111**, 877-946. (An influential review of the use of potential temperature as a vertical coordinate and potential vorticity as the central variable in atmospheric dynamics)

Hoskins, B.J., 1991: Towards a PV-θ view of the general circulation. **Tellus**, **43AB**, 27-35. (A pioneering attempt to apply the PV-θ-view to the general circulation)

Dritschell, D.G., and M.E. McIntyre, 2008: Multiple Jets as PV Staircases: The Phillips Effect and the Resilience of Eddy-Transport Barriers. **J.Atmos.Sci**., **65**, 855-874.

Edouard, S., R. Vautard and G. Brunet, 1997: On the maintenance of potential vorticity in isentropic coordinates. **Q.J.R.Meteorol.Soc**., 123, 2069-2094. (Well-written paper on the potential vorticity distribution and how it is established)

Eliassen, A, 1987: Entropy coordinates in atmospheric dynamics. **Zeitschrift für Meteorologie**, 37, 1-11. (A review of the origin and history of the use of potential

temperature as a vertical coordinate, written by one of the greatest dynamical meteorologists of the twentieth century)

Kleinschmidt, E., 1951: Über aufbau und entstehung von zyklonen. 1 Teil. **Meteorol.Rundschau, 3**, 1-6. (A pioneering paper, presenting the concept of potential vorticity inversion).

Thorpe, A.J., 1993: An appreciation of the meteorological research of Ernst Kleinschmidt. **Meteorol.Zeitschrift, N.F. 2**, 3-12. (Explaining the importance of Kleinschmidt's work, which was unfortunately not appreciated during his lifetime).

Thorpe, A.J., 1985: Diagnosis of balanced vortex structure using potential vorticity. **J.Atmos.Sci**., **42**, 397-406. (Detailed account of numerical method used to solve PV-inversion equation)

Thorpe, A.J., 1986: Synoptic scale disturbances with circular symmetry. **Mon.Wea.Rev**., **114**, 1384-1389. (Source of some important figures, which are discussed in the "classical" review paper by Hoskins, McIntyre and Robertson).

List of problems (chapter 7)

This is the April 2020 edition of chapter 7 (first written in 2011) of the lecture notes on Atmospheric Dynamics, by Aarnout van Delden (IMAU, Utrecht University, Netherlands, a.j.vandelden@uu.nl).

http://www.staff.science.uu.nl/~delde102/AtmosphericDynamics.htm